
Master thesis : Speeding Up Simulation-Driven Design for a High-Speed Planing Boat

Auteur : Ahmed, Osama

Promoteur(s) : 18531

Faculté : Faculté des Sciences appliquées

Diplôme : Master : ingénieur civil mécanicien, à finalité spécialisée en "Advanced Ship Design"

Année académique : 2021-2022

URI/URL : <http://www.auto-plan.net/>; <http://hdl.handle.net/2268.2/16562>

Avertissement à l'attention des usagers :

Tous les documents placés en accès ouvert sur le site le site MatheO sont protégés par le droit d'auteur. Conformément aux principes énoncés par la "Budapest Open Access Initiative"(BOAI, 2002), l'utilisateur du site peut lire, télécharger, copier, transmettre, imprimer, chercher ou faire un lien vers le texte intégral de ces documents, les disséquer pour les indexer, s'en servir de données pour un logiciel, ou s'en servir à toute autre fin légale (ou prévue par la réglementation relative au droit d'auteur). Toute utilisation du document à des fins commerciales est strictement interdite.

Par ailleurs, l'utilisateur s'engage à respecter les droits moraux de l'auteur, principalement le droit à l'intégrité de l'oeuvre et le droit de paternité et ce dans toute utilisation que l'utilisateur entreprend. Ainsi, à titre d'exemple, lorsqu'il reproduira un document par extrait ou dans son intégralité, l'utilisateur citera de manière complète les sources telles que mentionnées ci-dessus. Toute utilisation non explicitement autorisée ci-avant (telle que par exemple, la modification du document ou son résumé) nécessite l'autorisation préalable et expresse des auteurs ou de leurs ayants droit.



Universität
Rostock



SOLENT
UNIVERSITY
SOUTHAMPTON



With the support of the
Erasmus+ Programme
of the European Union



FRIENDSHIP SYSTEMS

Speeding-Up Simulation Driven Design for High-Speed Planing Boat

Submitted on August 24, 2022

by

AHMED Osama | Heinrich Mann Alle 7 | 14473 |

osama.ahmed@eleves.ec-nantes.fr

Student ID No.: 2105560

Supervised by: Dr.-Ing. Stefan HARRIES

Managing Director

FRIENDSHIP SYSTEMS AG

First Reviewer:

Dr. David LE TOUZE

LHEEA / Centrale Nantes

1 rue de la Noë

44321 Nantes cedex 3

France

Second Reviewer:

Dr. Lionel GENTAZ

LHEEA / Centrale Nantes

1 rue de la Noë

44321 Nantes cedex 3

France



Master Thesis

Abstract

In simulation-driven designs (SDD), the design optimization is frequently performed by standard Design of Experiment (DOE) or by using deterministic optimization strategies. This requires many designs to be tested depending upon the number of design variables present in the parametric model. This method is often too time-consuming or too expensive, mostly due to the complexity of industrial applications. Often high computational resources are required to determine the objective function. In this thesis, the idea is to present different methods for the faster turn-around times of SDD and apply it to the design and optimization of planing hull. The objective for the optimization is to minimize the overall resistance for the hull. The motion and forces acting on the hull are determined by Computational Fluid Dynamics (CFD), using Simcenter STAR-CCM+, the results of which are validated against experimental data. The difficulties of numerical modelling of planing hull includes the mesh deformation due to the large motion of the hull and the challenge of possible numerical ventilation due to inappropriate mesh near the boundary. The former is overcome by using a dynamic overset grid and the latter by using VOF-Slip velocity method. A thorough grid dependency study was undertaken in order to identify the best compromise between simulation time and accuracy. A fully parametric model was built in process integration and design optimization (PIDO) environment CAESES, and the design optimization is carried out by connecting it to the CFD solver in batch mode. The complete process of design optimization is automated to test several designs. The number of designs to be tested are vastly reduced by dimensionality reduction of the design space using Karhunen-Loeve Expansion (KLE), a dedicated Principal Component Analysis (PCA). The tested designs are used to train and employ a Surrogate Model, which produces optimized design variants based on the previous designs data. The comparison of different strategies against the conventional SDD method is shown, for the time required to get an optimized design along with the subsequent quality of obtained result. It is presented that by using AI-based optimization strategies and appropriate CFD simulation settings, the method of SDD can be made faster by a considerable amount of time.

Keywords: Simulation-driven Design (SDD); Parametric Modeling ; Parameter Reduction ; Karhunen-Loeve expansion (KLE) ; Computational Fluid Dynamics ; Planing Hull ; High-Speed Craft ; Volume of Fluid (VOF) ; Machine Learning

Acknowledgements

I would like to take this opportunity to express my sincere gratitude to all the people, especially my parents, family, friends, colleagues, supervisors and teachers who made it possible for me to reach this phase of my life.

Making this thesis would not be possible without the aid of my thesis supervisor, Dr.-Ing. Stefan Harries from Friendship Systems because of his valuable insights and instructions. I would also like to thank the complete team of Friendship Systems who welcomed me with open arms and guided me throughout the tenure. Special thanks to Claus Abt, Dr.-Ing. Sebastian Uharek, Carl Benz, Heinrich von Zadow, Carsten Fütterer, Mattia Brenner, Stefan Wunderlich and the whole team of Friendship Systems.

Very much gratitude to the team of Siemens Industry Software, Dejan Radosavljevic and Miles Wheeler. For providing the computational resources and licenses of STAR-CCM+ for CFD computations. Not only that, but also providing their valuable suggestions and recommendations throughout this work. Completion of this research work would not be possible without their help.

The whole team of AutoPlan project, Nalan Erol from UZMAR Shipyards, Turkey. Prof. Dr.-Ing. Andrés Cura Hochbaum and Matthias Volkmann from Technische Universität Berlin. Thank you for providing technical and practical information for validation purpose of this project.

Thank you to all the teachers from University of Liège and École Centrale de Nantes, for providing me with the knowledge to apply in the practical industrial applications and complete this thesis work. Indeed, the knowledge gained throughout my master's journey will help in excelling in my career further.

Lastly, I would like to extend the gratitude towards EMSHIP coordinator, Professor Philippe Rigo and Ms. Christine Reynders from International office, for giving me this auspicious chance for pursuing this master and providing me technical as well as administrative support and motivation throughout my master's journey.

Parts of the work presented in this thesis were realized within the research and development project AutoPlan, funded by the Federal Ministry for Economic Affairs and Climate Action (BMWK) on the orders of the German Bundestag and PtJ as the conducting agency within the MarTERA program of the EU (FKZ 03SX523A). For details see "www.auto-plan.net"

Declaration of Authorship

I declare that this thesis and the work presented in it are my own and have been generated by me as the result of my own original research.

Where I have consulted the published work of others, this is always clearly attributed.

Where I have quoted from the work of others, the source is always given. With the exception of such quotations, this thesis is entirely my own work.

I have acknowledged all main sources of help.

Where the thesis is based on work done by myself jointly with others, I have made clear exactly what was done by others and what I have contributed myself.

This thesis contains no material that has been submitted previously, in whole or in part, for the award of any other academic degree or diploma.

I cede copyright of the thesis in favour of the Ecole Centrale de Nantes (ECN), France.

Date: 23-Aug-2022

Signature: Osama Ahmed

Contents

List of Figures

List of Tables

1	Introduction	1
1.1	Literature Review	2
1.2	Motivation and Objectives	5
2	Theoretical Background	7
2.1	Principle of High-Speed Planing Craft	7
2.1.1	Geometrical Features	7
2.1.2	Working Principle	11
2.2	Numerical Methods	12
2.2.1	VOF - Slip Velocity Method	12
2.2.2	Body Force Propeller Method	15
2.3	Optimization and Dimensionality Reduction	17
2.3.1	Karhunen - Loève Expansion	18
2.3.2	Machine Learning based Optimization	20
3	Methodology	22
3.1	Geometrical Features & Parametric Modeling	22
3.1.1	Parametric Model	23
3.2	Computational Modeling	24
3.2.1	Mesh Discretization	24

3.2.2	Numerical Setup	27
3.3	Automated Software Connection	30
3.4	Speeding-up CFD Computations	32
3.5	Optimization Runs	33
4	Results and Discussion	35
4.1	Verification and Validation	35
4.1.1	Grid Convergence Studies	36
4.1.2	Quantification of Grid Uncertainties	37
4.1.3	Validation Studies	38
4.2	First Optimization Study	40
4.3	Numerical Model Adaptation	42
4.3.1	LCG Sensitivity Analysis	43
4.3.2	Effect of Appendages	44
4.3.3	Effect of Mesh Refinement	45
4.4	Optimization Runs	46
4.4.1	Design of Experiment (SOBOL)	46
4.4.2	Deterministic Tangent Search (T-search)	48
4.4.3	Surrogate Modeling	49
4.4.4	KLE based Optimization	52
4.5	Comparison of Obtained Results	54
4.5.1	Optimization Results for Simplified Model	54
4.5.2	Optimization Gain for Appended Model	57
5	Conclusion & Future Work	59
5.1	Future Work	60
	Appendices	63
A	Numerical Setup	64

B	Flowchart for PCA	66
C	Wave Forcing Equation	67
D	Convergence Histories	68
E	Correlation Plots	70
F	Optimized Designs	72
G	Baseline Results at Design Speed	77
H	Data Filtering	79
I	Validation Studies for 1st Variant (New Baseline)	80
J	Propeller-Open Water Characteristics	82

List of Figures

1	<i>Process Flow Diagram for SDD of Planing Hull</i>	2
2	<i>High Speed Planing Boat in working condition (https://mboat.eu/planing-hull/)</i>	4
3	<i>Deadrise Angle and its effect</i>	8
4	<i>Spray Rails in Planing Boat</i>	9
5	<i>Keel line Depth for Planing Boat</i>	9
6	<i>Chine for Planing Boat</i>	10
7	<i>Tunnel for Planing Boat</i>	11
8	<i>Fluid forces on an Inclined Plate(Bertram 2012)</i>	11
9	<i>Flow distribution around an Inclined Plate(Bertram 2012)</i>	12
10	<i>Calculation of Slip Velocity using concept of a Rising Bubble(Wheeler, Ryan, et al. 2021)</i>	13
11	<i>Blending Direction on Overset Mesh</i>	14
12	<i>Slip Velocity Vector representation with Blending Direction</i>	14
13	<i>Volume of fraction of Water, Numerical Ventilation beneath Hull</i>	15
14	<i>Volume of fraction of Water, Removal of Numerical Ventilation beneath Hull</i>	15
15	<i>Appended Hull modeled with Actuator Disk</i>	16
16	<i>Pressure Distribution of an appended hull with propeller disk</i>	17
17	<i>Two dimensional data in design space</i>	19
18	<i>Finding Principal Axis left, Principal Axis 1 on right</i>	20
19	<i>ANN Representation (Coursera - Deep Learning Specialization)</i>	21

20	<i>Defining Geometrical Features for Parametric Model</i>	23
21	<i>Complete Parametric Model</i>	24
22	<i>Overset Grid near Ship</i>	25
23	<i>Working of Overset Grid with Adaptive Mesh Refinement</i>	26
24	<i>Adaptive Mesh Refinement for free surface</i>	26
25	<i>Mesh Domain before & after Free Surface Refinement</i>	27
26	<i>Wall $y+$ values on the hull surface</i>	28
27	<i>Wave Forcing Zones and Boundary Conditions - Top View</i>	28
28	<i>Wave Forcing Zones and Boundary Conditions - Side View</i>	29
29	<i>Process Flow Diagram for SDD of Planing Hull</i>	30
30	<i>Automated Software Connection Convergence Histories</i>	31
31	<i>Automated Software Connection Convergence Histories Monitors</i>	31
32	<i>Velocity Plot to reach design speed</i>	33
33	<i>Pitch Plots with original and modified Inertia values</i>	33
34	<i>Hierarchical View of Optimization Runs</i>	34
35	<i>Grid Convergence Studies for motions and forces</i>	36
36	<i>Computational Time of different Grids</i>	37
37	<i>Uncertainty Quantification for Drag Force</i>	38
38	<i>Uncertainty Quantification for Pitch and Heave</i>	38
39	<i>Validation for Drag Force against Experiments</i>	39
40	<i>Validation for Pitch and Heave against Experiments</i>	39
41	<i>Old and New Tunnels Geometries</i>	40
42	<i>Free Surface around wake for Old Tunnel Geometry</i>	41
43	<i>Free Surface around wake for New Tunnel Geometry</i>	41
44	<i>Pressure Distribution for old and new tunnel geometries</i>	42
45	<i>LCG Sensitivity Analysis</i>	44
46	<i>Design of Experiment Analysis (SOBOL) - Correlations Plots</i>	47
47	<i>Design of Experiment Analysis (SOBOL)</i>	47

48	<i>Deterministic Optimization - Tsearch from best design</i>	48
49	<i>Performance of Machine Learning Model - Data Filtering</i>	49
50	<i>Surrogate based Tsearch - Comparison</i>	51
51	<i>Response Surface Optimization (DAKOTA)- Comparison</i>	52
52	<i>Design of Experiment of Reduced (KLE) Model</i>	53
53	<i>T-search from various designs - Using Surrogate Model</i>	54
54	<i>Comparison of two designs from T-search - Front View</i>	55
55	<i>Best Optimized Design Candidate - Using DAKOTA Response Surface</i>	58
56	<i>Best Optimized Design Candidate - Side View</i>	58
57	<i>Best Optimized Design Candidate - Bottom View</i>	58
58	<i>Flowchart of the steps of PCA</i>	66
59	<i>Convergence Histories for Drag Force</i>	68
60	<i>Convergence Histories for Pitch and Heave</i>	68
61	<i>Design of Experiment Analysis (SOBOL) - Correlations Plots</i>	70
62	<i>Design of Experiment Analysis (SOBOL) - Correlations Plots</i>	71
63	<i>Design of Experiment Analysis (SOBOL) - Correlations Plots - KLE</i>	71
64	<i>1st Optimized Design</i>	72
65	<i>1st Optimized Design - Side View</i>	72
66	<i>1st Optimized Design - Bottom View</i>	72
67	<i>2nd Optimized Design</i>	73
68	<i>2nd Optimized Design - Side View</i>	73
69	<i>2nd Optimized Design - Bottom View</i>	73
70	<i>3rd Optimized Design</i>	74
71	<i>3rd Optimized Design - Side View</i>	74
72	<i>3rd Optimized Design - Bottom View</i>	74

73	<i>5th Optimized Design</i>	75
74	<i>5th Optimized Design - Side View</i>	75
75	<i>5th Optimized Design - Bottom View</i>	75
76	<i>6th Optimized Design</i>	76
77	<i>6th Optimized Design - Side View</i>	76
78	<i>6th Optimized Design - Bottom View</i>	76
79	<i>Free Surface around the vessel</i>	77
80	<i>Free Surface around the vessel</i>	77
81	<i>Free Surface around the vessel</i>	78
82	<i>Pressure distribution with propeller disk</i>	78
83	<i>Validation Studies New Variant - Resistance</i>	80
84	<i>Validation Studies New Variant - Pitch</i>	81
85	<i>Validation Studies New Variant - Heave</i>	81
86	<i>Propeller Open Water Experimental Curves</i>	82

List of Tables

1	<i>Design Parameters Full & Model Scale</i>	23
2	<i>Grid Convergence Studies Parameters</i>	37
3	<i>Grid Uncertainty Quantification Values</i>	37
4	<i>Validation at Design Speed</i>	39
5	<i>Comparison of the old and new tunnel</i>	41
6	<i>Validation with Propeller Method</i>	42
7	<i>LCG Sensitivity Analysis</i>	43
8	<i>Effect of Appendages on Designs Performance</i>	45
9	<i>Effect of Mesh Size on Designs Performance</i>	45
10	<i>Kriging and Artificial Neural Network (ANN) Performance - Filtered Data</i>	50
11	<i>Principal Component Analysis , Captured Variance</i>	53
12	<i>Validation of Surrogate-Based T-search with CFD</i>	55
13	<i>Optimization Results for Simplified Model</i>	57
14	<i>Optimization Results for Fully Appended Model with Fine Mesh</i> . . .	58
15	<i>Validation Studies at different Speeds</i>	69
16	<i>Unfiltered Data for Surrogate Model</i>	79

Chapter 1

Introduction

Simulation-Driven designs (SDD) is the term often used in literature to describe the design optimization of a product by using several simulations. More often, designers create a digital-twin of the product and try to reduce the associate cost related to either operations or manufacturing of the desired product. The optimization process on the one hand can give a well working optimized product. On the other hand, the creation of digital-twin and the subsequent cost of several simulations can be very high and can sometimes overshadow the gain acquired through optimization. It can also vary with the application of the product, mass production vs personalized design and life cycle of the product. In all of these cases, the optimization is limited by the available computational resources. Carefully choosing the optimization strategies, objective functions and high-fidelity simulation strategies with the combination of data-driven methods can significantly improve the turn-around time of SDD. The idea of this thesis is to extend the previously carried out work in the area of SDD (as described in later section) to the marine application of High-Speed planing boat.

The application part of this work is related to free surface hydrodynamics problem of planing hull. Significant portion of the marine and ship design optimization are devoted to studying full displacement hulls because of their large applications and usage. Displacement ships are categorized with low Froude Number ($Fr < 0.3-0.4$). Most of the container and cruise ships lies in this range and thus research were carried out using Computational-Fluid Dynamics and tank testing to optimize this type of problem for better energy efficiency. However, for applications where high speed is desirable ($Fr > 0.8-1$) such as, pilot boats, naval and war ships. The optimization studies are limited for planing vessels due to the complexity of resolving flow around them, which involves high motions and turbulence. Having said that, with the current technological advancement in the field of CFD and high-performance

computing. The computational modeling and thus optimization of high-speed vessels by testing several designs can be made possible.

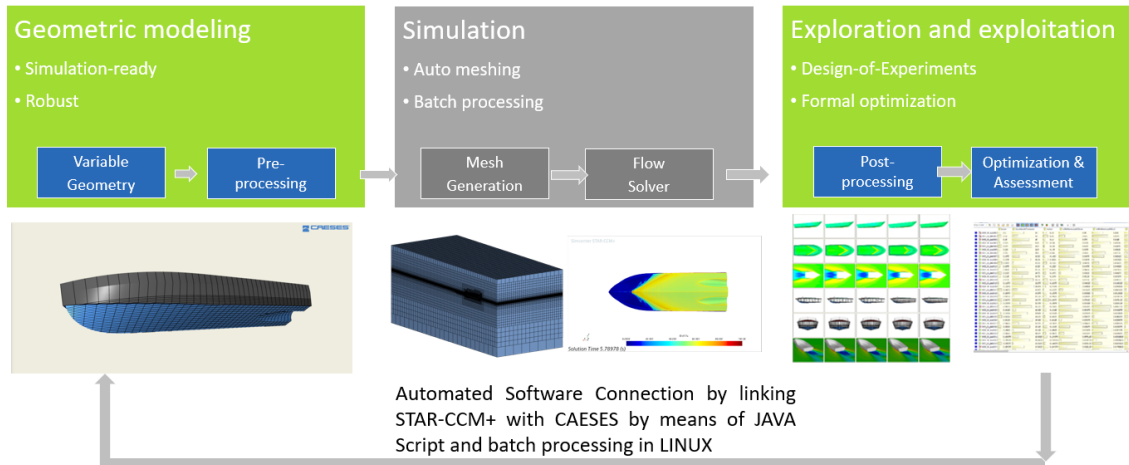


Figure 1: *Process Flow Diagram for SDD of Planing Hull*

The current work is dedicated to accurately modeling such type of Dynamic Fluid Body Interaction (DFBI) problem with Computational-Fluid Dynamics (CFD) code Simcenter STAR-CCM+. For this purpose, fully parametric model of the hull is built in Process Integration and Design Optimization (PIDO) environment, CAESES. After that, a software connection by means of Java-Script and extended macros was built between the two software to carry out different optimization runs in batch mode. Before carrying out the optimization run, the CFD setup was validated against the data obtained through the tank tests carried out in Technische Universität Berlin. For the optimization, different deterministic, stochastic and data-driven models are used. Subsequent potential of design improvement with respect to speeding-up the turn-around time is shown. Figure 1 highlights the process workflow for this work, the complete methodology and obtained useful results are presented and discussed in the later chapters.

1.1 Literature Review

In Computer Aided Design (CAD) and optimization, parametric modeling is the process of defining a CAD geometry with a few but interlinked variables, called design variables. For any parametric model, the success of the optimization depends on the quality of the parametric model, Harries 2015. In the optimization run, the design variables are thus varied and the effect of them on the objective function is calculated. Parametric modeling can be categorized in two groups, fully-parametric modeling (FPM) and partially-parametric modeling (PPM). In FPM, the entire geometry is built from scratch with the output as a CAD model governed completely

by input design variables. While in PPM, only the changes from an existing CAD model called baseline, is introduced using some parameters or design variables. Different types of partial parametric modeling techniques are Free-form Deformation (FFD), Radial Basis Functions (RBF), Mesh Morphing and many others are available. Thorough discussions for these models are given in Harries, Abt, and Brenner 2019.

The application of the Radial Basic Functions (RBF) approach for the design optimization of a Catamaran is presented by Harries and Uharek 2021. RBF functions allows defining so called sources and targets on the baseline geometry. These can be surfaces, points or curves defining the existing features on the baseline and intended new shape. The paper suggests the use of dimensionality reduction techniques such as Principal Component Analysis (PCA) to reduce the degree of freedoms. Since the reduction of design space comes at the cost of variability loss, the application of PCA to the given problem should be treated with care.

Various techniques and methods to study Simulation-Driven designs by means of fully or partially parametric models and Computational Fluid Dynamics has been studied in the last few decades. Specific applications and potential of it in the maritime industry is given by Zadow et al. 2019, in which the holistic ship design approach for the RoPAX ferry is presented. The work highlights the use of response surfaces for optimization, also called as Surrogate Models which are helpful and efficient at the early design stage of the vessel. Harries and Abt 2019a also discusses the Process Integration and Design Optimization (PIDO) environment software CAE-SES, on the application of HOLISHIP project. The workflow and approach using the integration of various computational tools can increase the turn-around time and reduces the time required to set-up the optimization manually in after each run.

Hasubek and Harries 2017 has shown the SDD for the Sailing Yacht and Motor Boat. Different flow analysis tools utilizing potential flow and RANSE methods were tested and potential for improvement was shown. It was highlighted that the reduction of resistance by 7% can be achieved at the design speed, by using a well-defined parametric model and appropriate flow simulation techniques. Similar work is given in Albert et al. 2016 , where the optimization using high-fidelity simulations is carried out and the use of cloud based computations to increase the turn-around time of the optimization process is suggested.

Harries and Abt 2019b have proposed the solutions for more and faster SDD by means of advanced parametric modeling, massive parameter reduction or Karhunen-

Loève Expansion (KLE), and parametric-adjoint simulations. The proposed solutions were applied on a duct for minimizing pressure loss across it, the potential of improvement in terms of pressure loss reduction and faster optimization time was shown. The extension of the given methods efficiently, using data-driven algorithms for the application on a more complex problem like flow optimization of high-speed planing hull is the context of this thesis.



Figure 2: *High Speed Planing Boat in working condition (<https://mboat.eu/planing-hull/>)*

The characteristics of hydrodynamic design of planing hulls is given by Savitsky 1964. It is one of the early work carried out in this domain. Savitsky presented empirical correlations useful for the determining lift, drag, wetted area and other parameters describing the performance of the vessel. The input for these relations are related to motion characteristics of the vessel such as, speed, trim angle, deadrise angle, and loading. These methods have proven to be useful for decades and are still in use at the early design stage but do not provide flexibility and adaptability to different modern designs.

The underlying principles and design methodology of the planing craft has been studied by various authors. Bertram 2012 presented the difference of planing hulls as compared to displacement hulls. In displacement hulls, the phenomenon is the direct application of Archimedes principle. In contrast for planing hulls, where the dynamic lift is generated by the action of fluid on the lower surfaces of the hull. For this example, parallels can be drawn with the inclined plate moving across fluid domain and the action of the fluid on it. Roshan et al. 2020 discusses about the Tunneled planing hull in calm water. It is shown that the tunneled planing hull is a special design of high-speed craft, which can reduce the frictional resistance of the hull and thus making it possible for the hull to achieve higher velocities.

High-speed planing crafts are designed for achieving high speed and thus they are usually lightly loaded with less draft. However, in some cases it may be needed to employ larger loads as compared to the design conditions. The effect of this condition on the operational performance on the planing hard-chine hulls is studied by means of numerical computations by Wheeler, Matveev, et al. 2021.

Difficulties in designing high-speed planing boats are determining the correct swimming conditions such as trim and rise of the vessel. These conditions directly affects the frictional resistance and propulsion power of the planing hull. Numerical modeling of this type of turbulent flow with large body motions requires very fine temporal and spatial resolution. Otherwise, mesh deformation near the body boundaries and numerical ventilation can occur. These phenomenon can influence the quality of the numerical results and thus increasing errors. Large errors can be avoided by using Dynamic Overset grid along with using VOF-Slip Velocity method as suggested in Wheeler, Ryan, et al. 2021.

Kim et al. 2013 carried out a test for performance improvement of planing hulls. Three designs were tested experimentally in calm water and in rough water sea states, for both resistance and seekeeping characteristics as objective function. The obtained results indicated that the best design for minimum propulsive power does not necessarily have to be the best design for see-keeping as well. In contrast, it can also go in two opposite directions for these two objective functions. Hence, the objective function should be chosen by considering the respective requirements for the vessel to be designed.

1.2 Motivation and Objectives

In previous section, the carried out work in the domain of Simulation-Driven Designs and Planing Hull designs is highlighted. Even though, both problems have been addressed by various authors separately. There is little to no knowledge of the combination of two, that is formal design and optimization procedure for such high-fidelity and complex CFD problem of planing hull.

The work presented here is part of the AutoPlan European Project. In this work, the idea is to perform the optimization of a planing hull. The optimization process here, to get the best design from simulations can be termed as Simulation-Driven designs. The optimization process follows formal Design of Experiment (DOE) and Exploitation involving various optimization techniques.

First, fully parametric model for the proposed design was made. The parametric model is termed as Baseline in the given context. Using the proposed loading condi-

tions and displacement of the vessel initial draft was then calculated. Given loading conditions also gives the current location of center of gravity, in each direction.

Secondly, 3D dynamic fluid body interaction problem of simulating high-speed planing hull was studied using Numerical computations. The output results were then verified and validated against the tank tests data. The numerical CFD model is then simplified for lower computational time by performing formal simplifications (removing appendages etc.) and by using advanced numerical techniques.

For such problem, large dynamic motions of trim and rise are the deriving phenomenon in determining the planing hull resistance. Therefore, as compared to displacement hulls for which resistance tests are mostly used both in CFD and tank tests. For high-speed boats, it is shown that the effect of propeller should be considered in the numerical computations to accurately predict equilibrium conditions.

Finally, the combination of above two setups was made using Java Script and CAESES (Process Integration and Design Optimization) PIDO environment. Formal Design of Experiment (DOE) and exploitation was carried out. The complete procedure of the design and optimization is automated in batch mode. HPC Cluster is used to perform computations by means of Linux based batch scripting. Obtained results highlights the potential of improvement with respect to the baseline design.

Design of Experiment (DOE) refers to taking random samples uniformly distributed around the parameter space to realize the potential of gain for optimization. While exploitation as the name suggests, is to use different optimization techniques and find a good minimum of objective function. As for 3D parametric model with various features, such as the example of planing hull. It requires the use of several design variables that eventually requires a larger sample size to explore the parameter space. Dimensionality Reduction of parameter space (PCA) is applied in the given context.

In the present work, the main motivation is to show the potential of improvement in the design and optimization turn-around time by means of using various CFD and optimization techniques, involving data-driven surrogate models. The objective function is the propeller thrust at the ship self-propulsion point and minimization of this objective function is the scope of this thesis.

This work pave the way for faster turn-around time of SDD for complex problems, requiring hundreds of hours of computational resources. The proposed methods and workflow can be applied to not only the design of planing hulls, but the process can be extended for faster design optimization of any high-fidelity problem that requires larger computational resources.

Chapter 2

Theoretical Background

This chapter discusses about different theoretical concepts that are used in the context of this thesis. It includes, principle of planing boat working, various numerical techniques used for efficient CFD modeling of planing craft in Simcenter STAR-CCM+. Furthermore, various theoretical remarks related to dimensionality reduction, optimization, data-driven surrogate models, are also some of the concepts introduced in this chapter.

2.1 Principle of High-Speed Planing Craft

As explained previously, for planing hulls the effect of dynamic lift balances the weight of the vessel which then comes out of water decreasing wetted surface area. This allows the boat to achieve higher speeds with relatively less coefficient of frictional resistance. However, to achieve this dynamic lift planing hulls uses different geometrical features which are dedicated to create this dynamic lift. These geometrical features and the working principle in terms of action of fluid on the bottom of hull is presented here.

2.1.1 Geometrical Features

For any conventional or displacement hull model, some of the geometrical characteristics remains fixed due to design constraints. These are typically the length, beam and design draft of the vessel. Although with these parameters fixed, designers often able to manipulate the other free variables to produce an optimized design with around 3-4 % reduction in the resistance (highlighted by different authors). With that being said, for the planing hulls there are some design components which dictates the planing characteristics and thus required power of the vessel. In this work,

these design variables are included in the parametric model as explained in later section. Here, some of these parameters and their effect on the vessel performance is shown.

Deadrise Angle:

Deadrise angle refers to the angle of V-section as seen from the front view in Figure 3. It is the driving factor for determining the generated lift for planing vessels. In displacement hulls, larger deadrise angles are often used as it provides better wave-piercing capabilities which dictates the sea-keeping capabilities of the vessel. As compared to planing hulls, which are flat-bottom rather than V-shape. The flat-bottom type vessels generates more dynamic lift from the action of fluid on the bottom of the hull, thus guiding the vessel out of the water and in to the planing regime. The generation of lift and the phenomenon of vessel coming out of the water can be seen in Figure 3.

As said above, to generate more dynamic lift it is desirable for the planing vessels to have smaller deadrise angles (flat-bottom). However, the decrease in the deadrise angles are often limited depending on the sea states in which the vessel has to sail. Very small deadrise angles can have good planing characteristics but can have undesirable sea-keeping characteristics. Therefore, a compromise should be made in between the two while designing planing hulls.

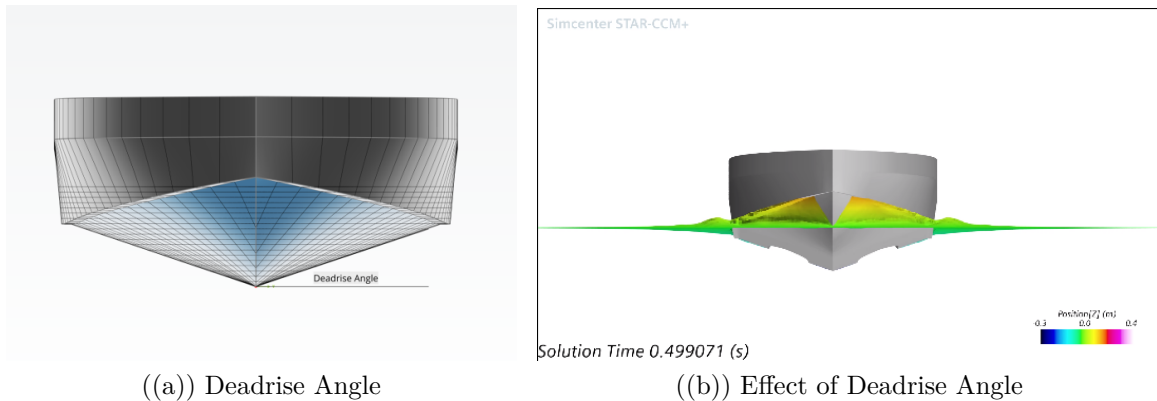


Figure 3: *Deadrise Angle and its effect*

Spray Rails:

Spray rails are located along with chine and they link bottom surface of the vessel with the deck. Most important feature of spray rails is to direct the fluid in the right direction and thus creating lift to make the hull rise. Re-direction of fluid downwards and backwards after the action on the vessel can be seen in Figure 3.

Figure 4 highlights the spray rails for the current baseline design. For some planing hulls, there can be additional spray rails at the bottom part to redirect the flow or to decrease the wetted surface area. The additional spray rails are out of the scope of this work.

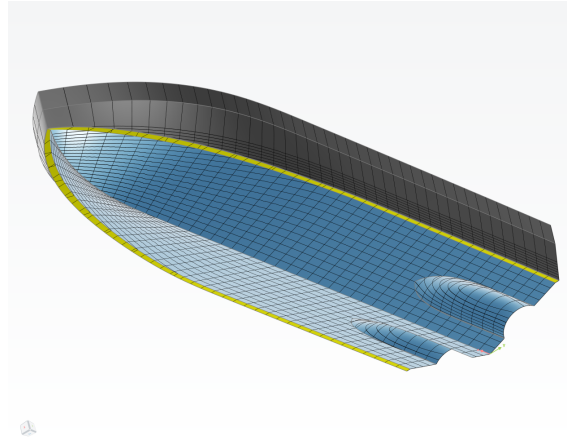


Figure 4: *Spray Rails in Planing Boat*

Keel line Depth:

For any vessel, keel line depth and its shape around bow part helps in determining its ability to move forward against the fluid. Planing vessels are mostly operated with less draft and thus large portion of bow remains out of water. Changing the convexity of keel line at the water line and beneath it, influence the bow shape and thus the performance of the planing hull. Figure 5 shows the employed keel line and bow shape for the baseline.

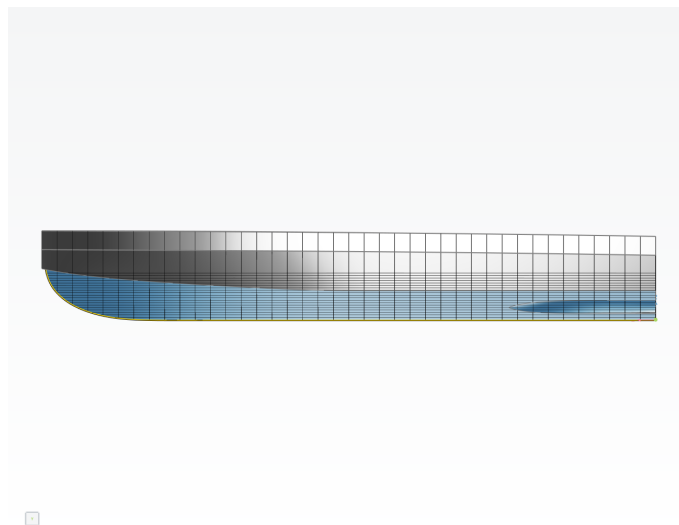


Figure 5: *Keel line Depth for Planing Boat*

Chine:

Just like any conventional hull shape, chine is the area which is at the intersection of bottom and sides. In Figure 6 it can be seen that the chine links the bottom with spray rails and thus eventually, the sides of the vessel. Hard-chine planing hulls push water out and away from the hull and thus making the vessel to enter planing regime at much lower speeds as compared to soft chine planing hulls. In this work, hard chine planing vessel with spray rails has been employed.

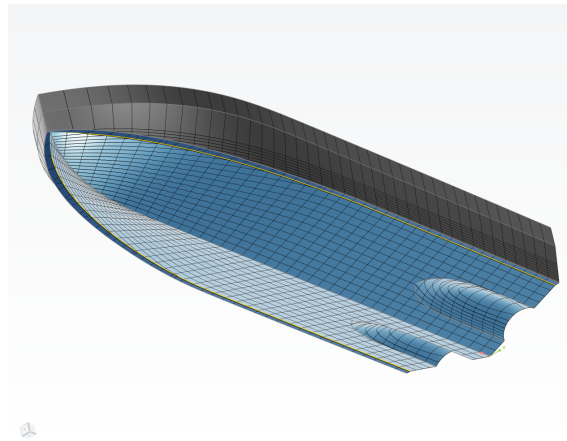
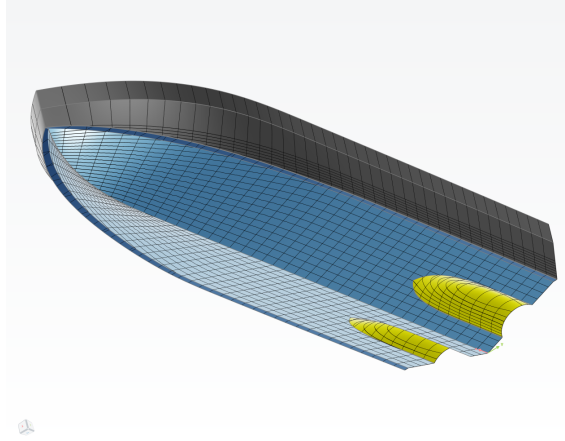


Figure 6: *Chine for Planing Boat*

Tunnel:

Initial designs of planing hulls have tunnels incorporated to reduce the hull draft, propeller noise and provide more flexibility in shaft and propeller placement. It allowed the vessel to be operated with smaller shaft angles, specially in the conditions where trim is larger. After that, the concept of stepped hull for high speed vessels was introduced. The idea of stepped hulls is to introduce one or more discontinuities at the hull bottom, increasing the flow separation and drag reduction. Tunneled planing hulls operates on the same principle, it provides better shaft angles and larger trim angle. Furthermore, the reduction of wetted surface area and corresponding drag is one more application of the tunnel in planing hulls.

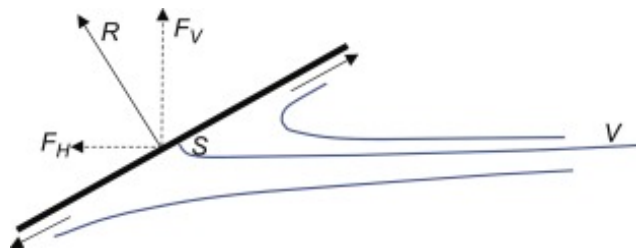
Figure 7 shows two tunnels as included in the baseline. Both of these tunnels have one propeller each, which makes the twin-screw propulsion system. Along with the hull form, the optimization of the tunnel as well is the scope of this thesis.

Figure 7: *Tunnel for Planing Boat*

2.1.2 Working Principle

After mentioning and defining about different features of the planing hulls and their functions. The following figures depicts the basic working principle of planing hulls by show-casing a simplified 2D inclined plate moving across the water.

In Figure 8 , the reaction forces resulting from the action of fluid on the inclined plate is shown. Horizontal component of the force F_H corresponds to the horizontal drag force the body will encounter while moving forward in the water. The vertical force F_V refers to the lift force acting on the vessel. While in displacement vessels the objective function is limited to minimizing Drag Force F_H . In planing vessels, the objective is to minimize the horizontal component of the force and maximize the lift force F_V of the planing vessel.

Figure 8: *Fluid forces on an Inclined Plate(Bertram 2012)*

For the more realistic depiction of this phenomenon, Figure 9 present the action of fluid and the corresponding velocity vectors. It can be seen that the generation of lift and horizontal drag force are function of the wetted length L_E and trim angle α . These two parameters also influence the center of pressure location underneath the hull.

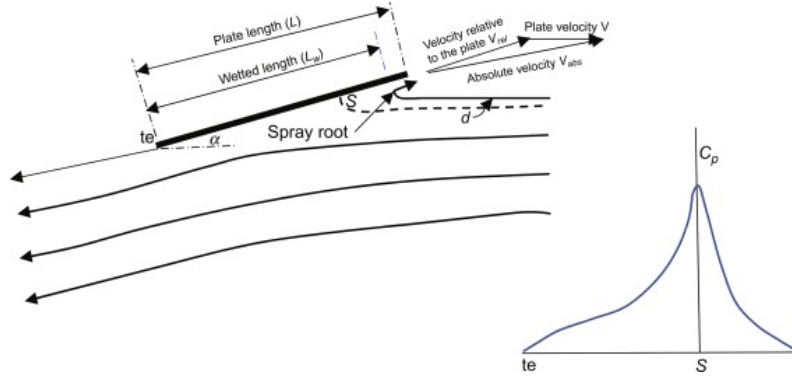


Figure 9: *Flow distribution around an Inclined Plate*(Bertram 2012)

Similarly, parallels can be drawn with the actual planing hull geometry. With the addition of some features that promotes the efficient use of the vessel. The basic principles of working of the high-speed planing craft remains same. That is, generation of additional dynamic lift to pull the hull out of water. Further, directing the flow in the right direction to promote the rise, and the use of additional geometrical features to decrease the wetted surface area beneath the hull.

2.2 Numerical Methods

Although various numerical methods are used which are briefly described in Methodology section, this section focuses on developing concepts about newly and efficiently employed methods in the current context. Some of them are, the concept of Slip Velocity to encounter numerical ventilation in CFD simulations. Also, the concept of body force propeller method, to simplify the effect of propeller forces and to include them in the computations is discussed here.

2.2.1 VOF - Slip Velocity Method

The concept of slip velocity is introduced in STAR-CCM+ and is used in this work. Thorough implementation and concept behind this work is given in Wheeler, Ryan, et al. 2021. The main idea for using VOF-Slip velocity method is to remove numerical ventilation beneath the hull.

Numerical ventilation is the phenomenon of having artificially entrapped air beneath the hull. It particularly effects the shear component of force near walls and it can arise due to smeared interfaces and improper time or spatial discretization. Conventional VOF models works well for immiscible flows with free surfaces. Particularly, for the applications where shape and position of interface (or free surface in this case) is fully resolved. The application of this method on planing hull requires very

high resolution in both time and space, thus making the simulations and subsequent optimization impractical. While in VOF method, the mixing of two phases is irreversible, Slip Velocity method allows the mixture to separate again and give meaningful results. The slip velocity can be defined as,

$$V_{PS} = V_S - V_P \quad (2.1)$$

Where, V_S is the velocity of the secondary phase and V_P is the velocity of the primary phase. The difference between the two will give the relative velocity between the two phases, termed as Slip Velocity. The slip relative velocity helps in recovering smeared interface between two phases. One of the approach of defining slip velocity is called, Drag-based approach. In this method, slip velocity is calculated based on the resultant of the forces acting on dispersed phase. These forces are, drag force, gravity or buoyancy force, and centrifugal force.

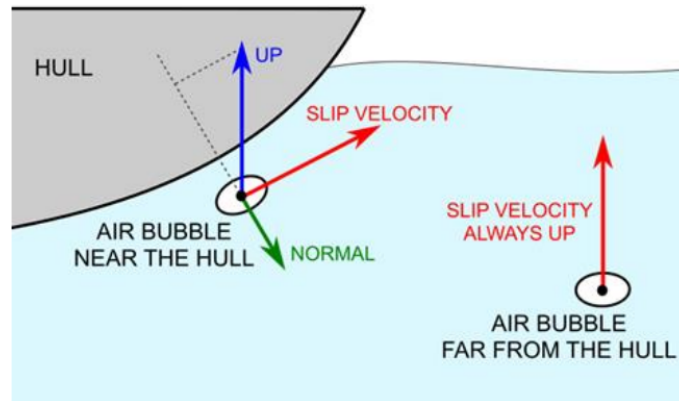


Figure 10: Calculation of Slip Velocity using concept of a Rising Bubble(Wheeler, Ryan, et al. 2021)

For marine applications, it has been observed that the use of drag-based slip velocity can be problematic for computational stability. The efficient method to define slip-velocity for marine applications is called User-defined Slip Velocity method. User defined function implemented in STAR-CCM+ for given application uses the concept of a rising air bubble suspended in water. As shown in Figure 10, in the far-field the bubble will rise due to the effect of buoyancy and defining vertical slip velocity. Near the body or hull, the component of slip velocity can be calculated by subtracting the surface normal mapped on the hull surface. These surface normal can be calculated from the volume mesh at each time step. Alternatively, to reduce the computational cost here, the slip-velocity is calculated after reaching the equilibrium floating condition.

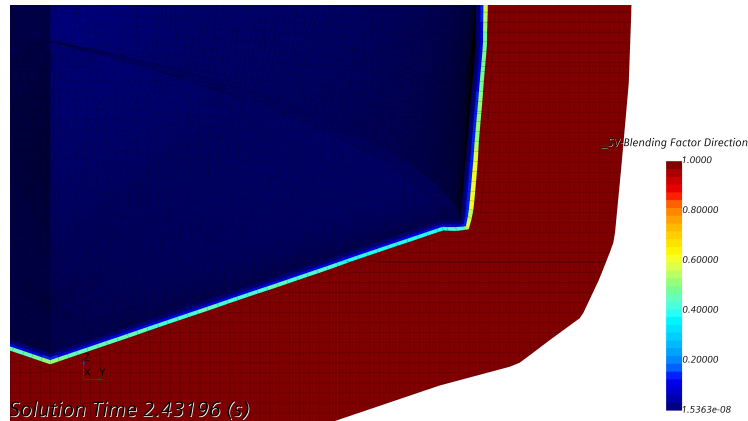


Figure 11: *Blending Direction on Overset Mesh*

Figure 11 shows the blending function which dictates the slip velocity direction. It is used to remove the normal component of the slip velocity. As can be seen, in the far-field the blend direction is 1. In contrast, it changes to 0 very close to the hull. A parameter blending distance B_d is the function of Prism Layer Thickness. The value of B_d influence the change between far-field and near-field. Further formulation about blending direction and different relevant formulae are given in Appendix A.

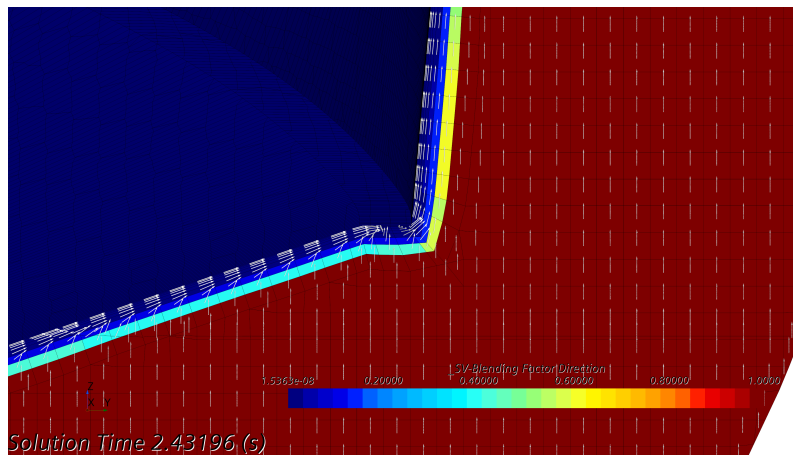


Figure 12: *Slip Velocity Vector representation with Blending Direction*

Figure 12 presents the results of the application of VOF-Slip Velocity method on given planing hull. The direction and magnitude of the shown vectors represent the direction and magnitude of slip velocity, respectively. These slip velocity vectors defines relative velocity between two phases and it can be used to recapture the phases separately from the mixtures. The following two figures, Figure 13 & 14 shows the presence of numerical ventilation and its removal.

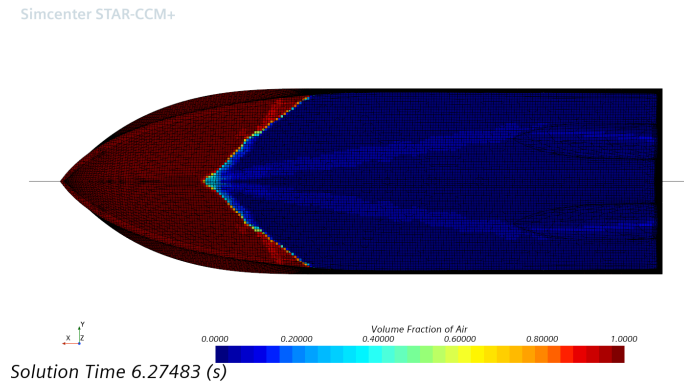


Figure 13: *Volume of fraction of Water, Numerical Ventilation beneath Hull*

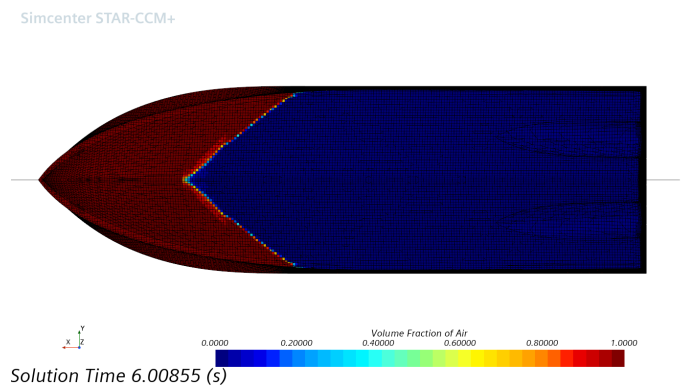


Figure 14: *Volume of fraction of Water, Removal of Numerical Ventilation beneath Hull*

2.2.2 Body Force Propeller Method

One of the initial findings of this work, highlights the importance of modeling propeller forces in order to correctly simulate planing hull. For displacement hulls, resistance tests are adequate in predicting the required power output in most of the cases. By using Froude scaling, model scale tests are usually performed in tank tests and the results are then extrapolated to full scale with minimal loss of accuracy. Similar methods can be used by using numerical tools like CFD. Furthermore, if enough computational resources are available, CFD results are usually obtained in full scale.

This method is not very efficient for planing hulls, due to its different working principle. Planing hulls often have lighter displacement, large dynamic trim and sinkage motions. Presence of propeller can directly effect the swimming conditions and thus wetted surface area of the vessel. In the context of optimization, it is essential to correctly identify the objective function as close as possible. Due to this fact, the propeller forces are model in simulations using Body Force Propeller

Method and the propeller thrust is chosen as the objective function.

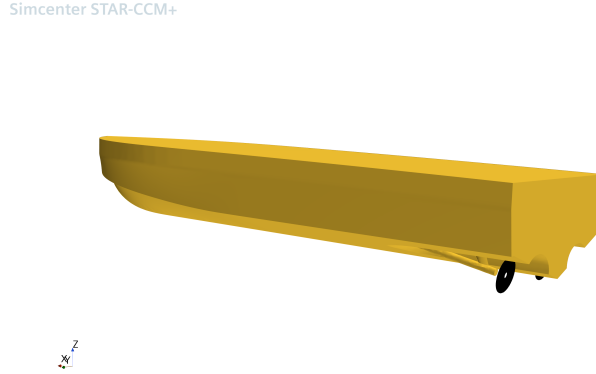


Figure 15: *Appended Hull modeled with Actuator Disk*

To model propeller forces in CFD simulations, there are two methods which are being used. First, complete propeller geometry can be resolved using very fine mesh size. This type of method predicts the propeller forces as well as local flow around propeller with good accuracy. However, this comes with the cost of very fine discretization in space and time with combination of sliding mesh. Second method is called Body Force Propeller Method, or sometimes called as Virtual Disk method. The idea behind this method is to simplify the propeller geometry in a circular virtual disk. This model adds a momentum source in momentum equation and approximate the average flow field around the propeller.

By using this simplification, propeller forces can be resolved with a relatively coarser mesh and without the need of sliding mesh around propeller geometry. To perform self-propulsion test, propeller open-water characteristics are required. Based on the propeller curves, and using fundamental equations for propulsion as in given equations, operating point is calculated. Equations 2.2 to 2.4 presents this formulation.

$$J = \frac{V_a}{n D} \quad (2.2)$$

$$K_T = \frac{T}{\rho n^2 D^4} \quad (2.3)$$

$$K_Q = \frac{Q}{\rho n^2 D^5} \quad (2.4)$$

In this project, body force propeller method is used to model the effect of propeller forces. Propeller characteristics are taken from experimental data available and

propeller thrust is taken as objective function to be minimized. Figure 16 presents the pressure distribution acting on the hull for this type of implemented model. From this figure, high pressure zone near the fore part depicts the point where free surface attaches to the hull. In planing hulls it is located near the midship and towards fore part of the vessel. Negative pressure near the aft part indicates lower pressure due to the suction effect of the propeller.

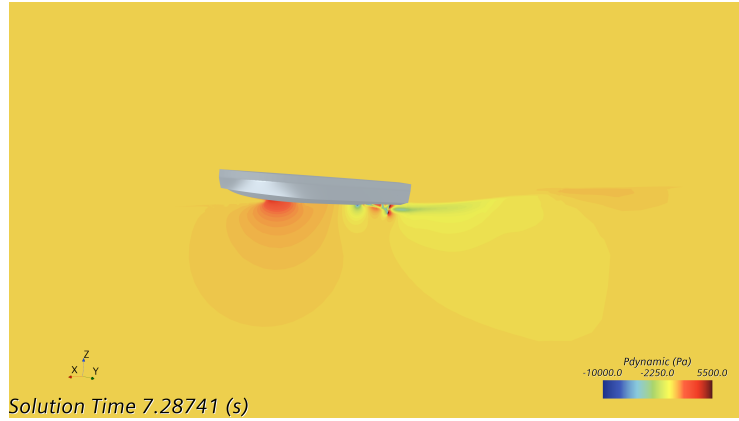


Figure 16: *Pressure Distribution of an appended hull with propeller disk*

2.3 Optimization and Dimensionality Reduction

Standard optimization procedures involves design variables and objective function. Design variables are the parameters that dictates the position or influence of each design feature (in this case hull parametric model). While objective function is the function to be optimized and often called as cost function. In marine industry, achieving higher energy efficiency has always been the desired cost function. Also, in the context of planing hulls it is desired to minimize the propeller thrust and thus engine power by diligently designing the propeller and tunnel.

Equation 2.5 depicts a standard optimization problem formulation to minimize the objective function $f(x)$. Equations 2.6 to 2.7 represents inequality and equality constraints on the objective function, respectively. Other than bounds on objective function, there can be bounds on design variables as well to incorporate manufacturing bounds. For example, design variable of pipe diameter can not be less than 0. Equation 2.8 presents the bound on design variables.

$$\min_{x_i} f(x) \quad (2.5)$$

$$s.t. \quad g_j(x) < 0 \quad j = 1 \dots m \quad (2.6)$$

$$h_k(x) = 0 \quad k = 1 \dots l \quad (2.7)$$

$$x_i \leq x_i \leq x_i \quad i = 1 \dots n \quad (2.8)$$

This section introduces two concepts that are involved in this work. First is called Karhunen - Loève Expansion (KLE) which is a special type of Principal Component Analysis used in dimensionality reduction of design space. Second concept is the use of data-driven and Machine Learning algorithms to increase the turnaround time of the optimization. The mentioned concepts corresponds to dedicated fields of their own and requires detailed study. Upcoming sections present brief concepts and their use for this work.

2.3.1 Karhunen - Loève Expansion

Principal Component Analysis (PCA) is a statistical procedure that has been used vastly to reduce large dimensional data and summarize it with few parameters. More often, the number of design variables for a parametric model is between 10-20 and occasionally can go up to 50. With the increase in design variables the number of designs to be tested to explore the design space also increases exponentially. For Design of Experiment (DOE), a rule of thumb is to have number of simulated designs equals to square of design variables (n^2) as given in Harries and Abt 2019b.

PCA should not be confused with regression analysis, which tries to find correlation between different design variables and objective function. Instead, the main principle is to project data points on to lower dimensional space. The projection is done such that to maximize the covariance of the data set to capture maximum variability of original data points. Standard covariance matrix for a 2D space has a following structure,

$$Covariance\ Matrix = \begin{vmatrix} Var(X) & Cov(X, Y) \\ Cov(X, Y) & Var(Y) \end{vmatrix} \quad (2.9)$$

More general form of covariance equation, also called Closed Form of Covariance Equation is given in equation 2.10 to 2.12. S denotes the covariance matrix while U_1 is the unit vector.

$$\max U_1^T \left[\frac{1}{N} \sum_{n=1}^N (X_n - \bar{X})(X_n - \bar{X})^T \right] U_1 \quad (2.10)$$

$$\max U_1^T S U_1 = f(x) \quad (2.11)$$

$$S.t \quad U_1^T U_1 = 1 \quad (2.12)$$

Other than reduction of design space, PCA also helps in data visualization of larger set, and feature extraction or determining dependency of different variables. The working of PCA can be defined in few steps. In order to understand better, consider two dimensional uncorrelated data as shown in Figure 17. The task is to reduce this two dimensional data into one dimensional space by using Principal Component Analysis.

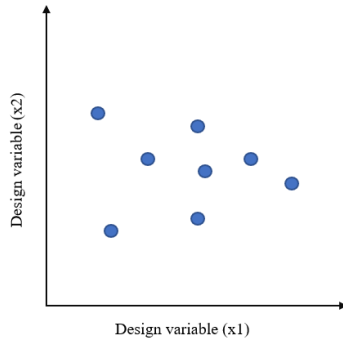


Figure 17: *Two dimensional data in design space*

First step in PCA involves data centering, axis of data points is shifted to centralize the data. While doing so, the co-relations between the data points remains same. Second step is to compute the covariance matrix of the high dimensional data and then trying to find an axis which maximizes the covariance when projecting the data onto it. To better visualize this step, the depiction of this step is given in Figure 18.

The axis which maximises the covariance is called Principal Axis. The principal axis is defined by its eigenvalue and eigenvectors, termed as principal parameter. While for 2D data there is only one principal parameter, for high dimensional data there can be many principal axes and thus parameters. These principal parameters denotes the design variables and CAD model in KLE space. All the principal axis are orthogonal to each other.

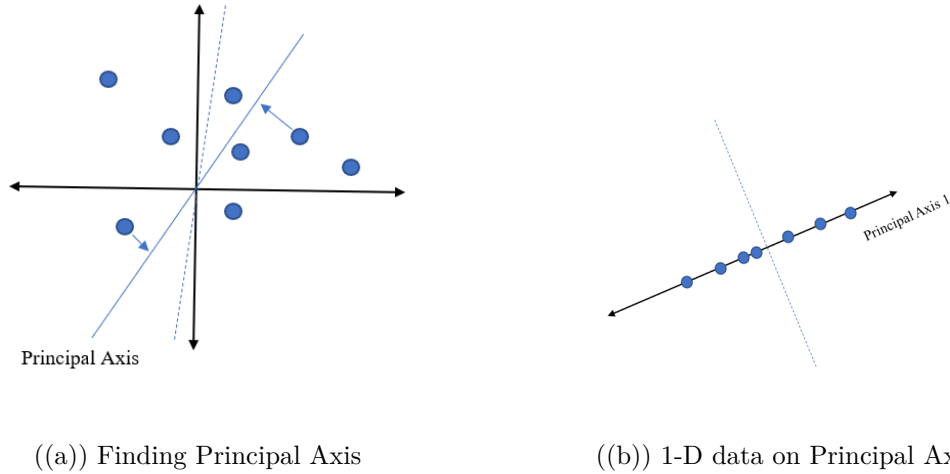


Figure 18: *Finding Principal Axis left, Principal Axis 1 on right*

From these principal parameters a handful of them are chosen so as to reduce the design space and achieve desired variability for the CAD model. Often, principal parameters are chosen to achieve 95% or more CAD variability. Application of PCA can be very useful while dealing with data or optimization with higher number of design variables.

Karhunen - Loève Expansion (KLE) is a particular type of PCA. It works by defining the CAD geometry in set of points distributed along its surface. These points now serve as the basis for dimensionality reduction. Input to KLE in the given context, is the number of points and number of samples. Number of points distributes the CAD into desired data points, while samples are generated to analyze the covariance matrix and its subsequent maximization. Since, it is only decomposition in CAD Space and evaluated functions are eigen values and covariances, this step is much faster.

After selecting desired principal parameters and captured variance, the KLE model needs to be transformed from KLE space to CAD Space to perform the evaluation of objective function using CFD. This process of transformation can be either Linear or by using SIMPLEX transformation. Flowchart describing the previously mentioned steps is given in Appendix B.

2.3.2 Machine Learning based Optimization

In this work, different surrogate models are built from the data generated from CFD Simulations. These machine learning models are then employed to perform optimizations using deterministic and stochastic methods. Some commonly used

surrogate models are, Linear Regression, Kriging and Artificial Neural Networks.

Kriging

Kriging Model is also called as deterministic interpolation method, because the value of the objective function is calculated directly from its surrounding values. For that, weights are assigned to each neighbor point and objective function at the new point is calculated using equation 2.13 and 2.14. Where, ϵ_{new} is the error of estimation for the newly estimated value.

$$y_{new} = W^T y + \epsilon_{new} \quad (2.13)$$

$$y_{new} = w_1 y_1 + w_2 y_2 + \dots + w_n y_n + \epsilon_{new} \quad (2.14)$$

Hence, only unknown for the kriging model is the calculation of weights 'W'. These weights are determined by Variogram fitting on the data points. Detailed explanation about it can be found in the literature. Following two equations are used for weight calculations in kriging model.

$$\gamma(x_i, x_j) = \frac{1}{2} (y_i - y_j)^2 \quad (2.15)$$

$$\gamma(x_i, x_j) W = \gamma(x_{new}, x_i) \quad (2.16)$$

Artificial Neural Networks

Artificial Neural Network is another type of Machine Learning model. Although, there are many modifications of the ANN for different data types. The basic principle is shown in Figure 19, the working of the ANN is similar to human brain where different neurons carries different weights. With the given inputs and outputs, the network works back and forth and train the model for prediction.

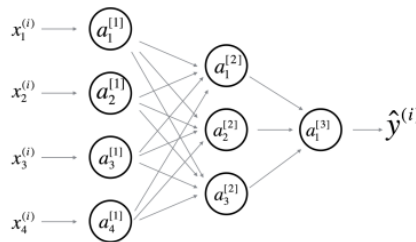


Figure 19: ANN Representation (Coursera - Deep Learning Specialization)

Chapter 3

Methodology

This section is focused on presenting complete methodology applied for this work. Starting from the geometrical features and parametric modeling, discussing concepts about computational modeling of the problem. Further, automation of the design optimization procedure is discussed. In the end, the concepts and methods of applying optimization runs and dimensionality reduction is presented.

3.1 Geometrical Features & Parametric Modeling

The starting baseline of this project is taken from an existing hull model available from UZMAR Shipyard. Using the available hull model, fully parametric model is then built in CAESES to depict the already built geometry. This CAD parametric model is termed as 'Initial Baseline' for this project. It has different geometrical features to improve planing characteristics and efficiency of the vessel, such as, Spray Rails, Chine and Tunnel.

Table 1 presents the features and design parameters for both full scale and model scale. Froude scaling with a scaling factor of $\lambda = 3.2871$ is used. Using Froude Similitude, the optimization is focused on model scale. The use of model scale dimensions for the optimization is backed by tank tests results, which are also performed with model scale dimensions. Design speed of 27.5 knots, corresponding to Froude number of 1.36 is the target speed for optimization studies. Attachment points represents the point of attachments in tank tests as well as simulated CFD computations.

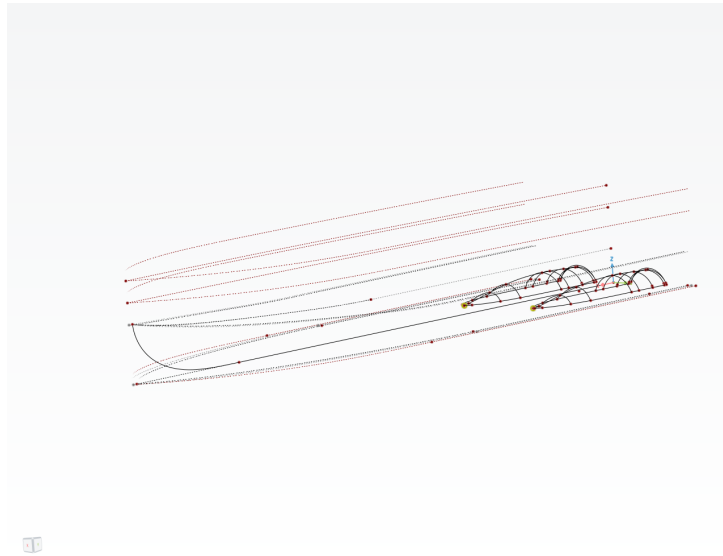
Table 1: *Design Parameters Full & Model Scale*

Parameters	Denotation	Full Scale	Model Scale	Units
Peak Length	Lpp	11.058	3.364	m
Beam	B	3.5	1.065	m
Displacement	Δ	9.5	0.267	ton
Draft	D	0.611	0.186	m
Longitudinal Center of Gravity	LCG	4.945	1.504	m
Vertical Center of Gravity	VCG	0.7	0.213	m
Speed	V	27.5	15.168	knots
Froude Number	Fr	1.358	1.358	
Attachment Point X	AP_x	5.529	1.682	m
Attachment Point Z	AP_z	0.611	0.186	m

3.1.1 Parametric Model

The idea of making parametric model is to represent the complete CAD geometry by intelligently defined few parameters. These parameters allows complete freedom to adapt the design within feasible design space, for the optimization runs.

While some of these parameters remains fixed for optimization, like length between perpendiculars L_{pp} and beam B of the vessel. Other remaining parameters called design variables, are allowed to change and changing these parameters gives different geometrical shape and thus design variants for the optimization.

Figure 20: *Defining Geometrical Features for Parametric Model*

In this case, a total of 18 design variables defines the planing hull model. These design variables can also be regarded as the degrees of freedom for the optimization studies. Figure 20 presents the geometrical curves and points that are used to

make the parametric model. Out of 18 design variables, 8 variables are defining the complete hull model except tunnel. This includes, transom, keel line, chine, spray rails and deck of the vessel. The other 10 variables are devoted to predict and define the tunnel model. As compare to the hull, the tunnel is more curvilinear and requires larger number parameters to completely defines it geometry.

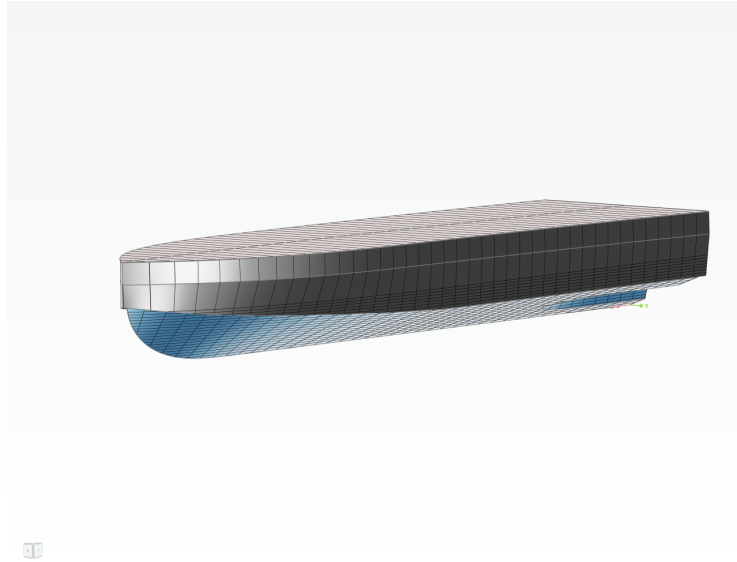


Figure 21: *Complete Parametric Model*

All of these curves and points are joined together by surfaces and make a complete CAD model as presented in Figure 21. The tunnel solid model is subtracted from the hull solid model using a Boolean operation, thus giving the required tunnel cavity for propeller mounting, beneath the planing hull.

3.2 Computational Modeling

Accurate prediction of dynamic motions and resistance for the planing vessels, requires distinctive numerical techniques than the conventional displacement vessel problem. It involves, using dynamic overset grids, adaptive mesh refinement, slip-velocity method, wave forcing zones and the use of adaptive time-step for accurate and faster CFD computations. Upcoming section presents these employed strategies and their implementations in the given context.

3.2.1 Mesh Discretization

For marine applications, there are different strategies to predict correct motion and resistance of the vessels. ITTC “International Towing Tank Conference” n.d. has documented these guidelines for different type of vessels simulations, as well as

guidelines for the practical implementation in the tank tests. Because of the highly turbulent (larger Reynold's number) problem for ship flows, getting meaningful results from CFD computations requires appropriate simulation settings.

Other than properties of water, Reynold's number is a function of characteristic length and speed of the vessel and is directly proportional to these values. For larger tanker and bulk carriers, the speed is limited and highly turbulent flows is mainly because of the larger peak length of the ship. For planing hull, although the length is limited but these vessels are designed to be operated with high speed and thus resulting in higher Reynold's number. A unique characteristic of high-speed planing vessel is that, it also has larger dynamic motions such as pitch and heave. To capture these motions and to accurately discretize free surface, dynamic overset grid motion along with free surface adaptive mesh refinement is used. The overset grid can be seen in Figure 22.

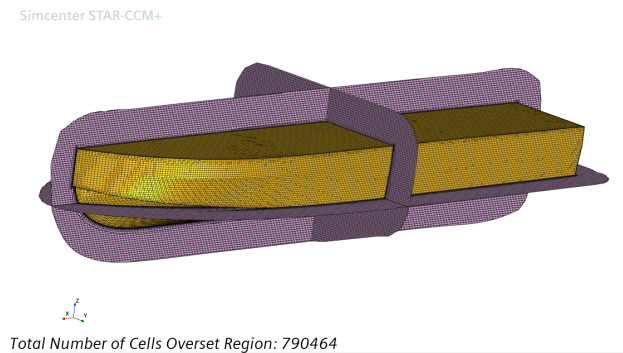


Figure 22: *Overset Grid near Ship*

The primary working of overset grid technique, known as Chimera Grid is to capture large motions and avoid mesh distortion in presence of large motions. It employs two separate grids, one for background mesh in which the cells lying at overset section are inactive. The other part is the overset grid around ship, this grid is responsible of capturing the boundary layer and maintaining required y^+ values using prism layer mesh. Information transferring between these two grids is done by overset algorithm. Proper implementation of this technique requires transitional domain between background and overset grid. Different transitional zones ensuring smooth transition of mesh size and adaptive refinement for overset grid are used. Figure 23 presents these domains at the final time-step of the solution.

Information transferring between two domains also requires an intersection zone. This overset intersection zone have few cells at the intersection of both domains and uses same cell size across each domain. Although the use of overset grid is very useful for bodies with larger motion, before using this type of technique all

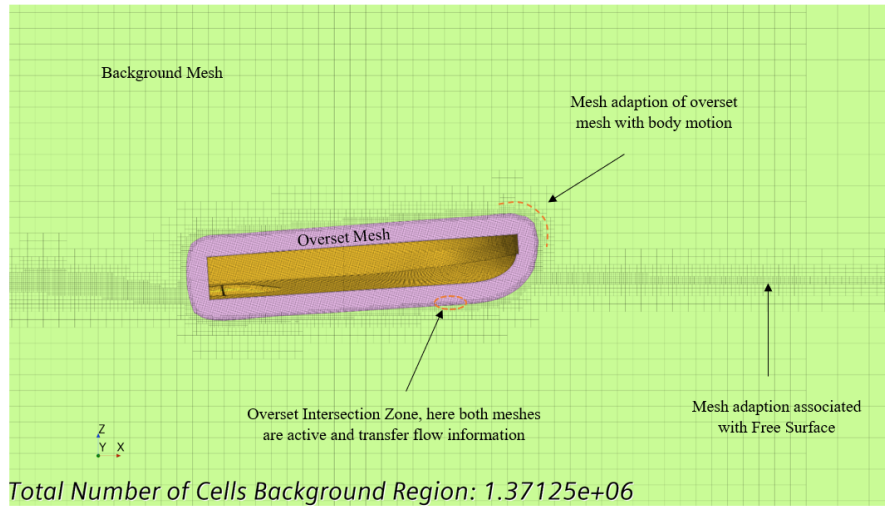


Figure 23: *Working of Overset Grid with Adaptive Mesh Refinement*

of the above mentioned requirements should be treated with care. In this project, tight over-set grid in combination with adaptive mesh refinement is used. Adaptive mesh refinement for overset grid ensures good transfer of motion between the two domains. Adaptive free surface refinement (AMR) is used to adapt the mesh size depending on the turbulence and flow conditions. By doing so, free surface is refined only in the required area as shown in Figure 24.

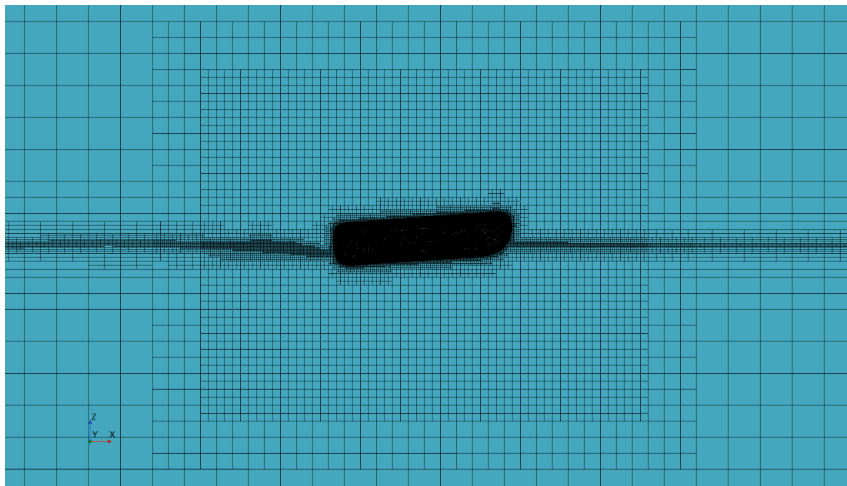


Figure 24: *Adaptive Mesh Refinement for free surface*

Figure 25 also shows the coarsen and refined free surface mesh. The imposed velocity in surge direction starts from zero and reaches the required design speed. Significance of using this type of imposed velocity is to avoid excessive pressure forces on the hull leading to numerical uncertainties. In the phase of increasing speed, free surface adaptive mesh refinement is not applied. It is applied just after reaching the design speed to accurately capture the flow.

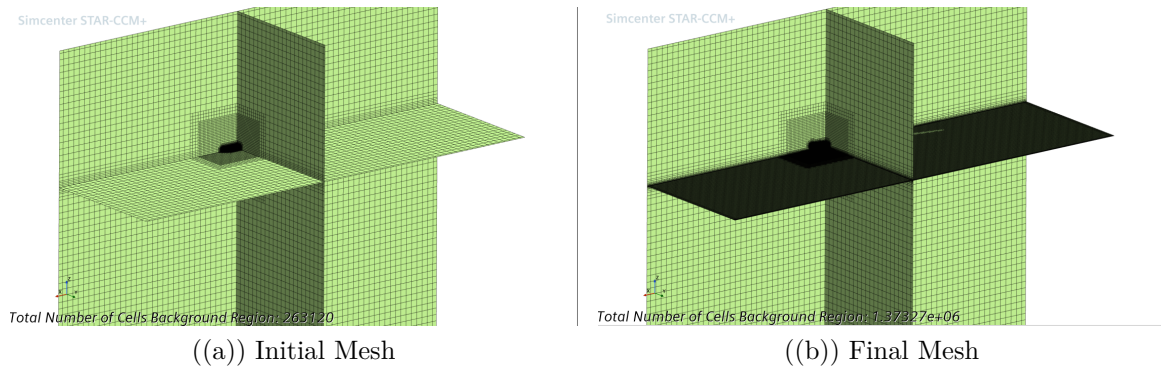


Figure 25: *Mesh Domain before & after Free Surface Refinement*

3.2.2 Numerical Setup

For the CFD computations, utilized physical setup can be briefly described in following points.

- Segregated Fluid solver for in-compressible fluids is used.
- Semi-Implicit Pressure Linked Equations (SIMPLE) scheme is used to couple velocity and pressure equations using 2^{nd} order convection schemes.
- In the transient acceleration phase while reaching the design speed, 1st Order Pseudo State Transient Solver is used in order to reach steady state operating conditions.
- Reynold's Averaged Navier Stokes (RANS) based Realizable K-Epsilon method with wall function approach is employed.
- Volume of Fluid (VOF) scheme to model free surface using HRIC (High Resolution Interface Capturing) scheme is used.

RANSE Model & Wall y^+

The prism layer thickness in the overset grid is kept constant to ensure constant y^+ values. Wall function approach with realizable K-epsilon as defined previously is utilized. Figure 26 shows the y^+ distribution beneath the hull at final steady state swimming conditions.

Boundary Conditions & Forcing Zones

For high speed vessels where hydrodynamic forces dominates hydrostatic contributions, appropriate method is to resolve motion using mass and inertia properties,

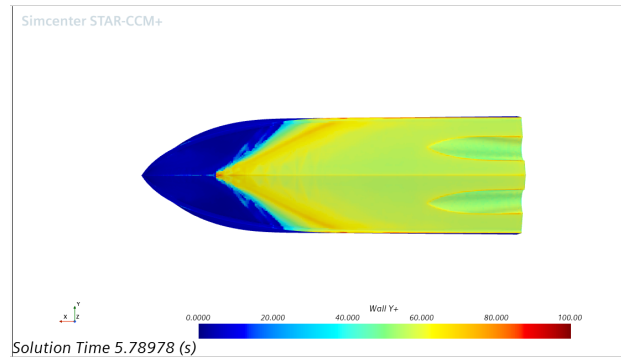


Figure 26: *Wall y^+ values on the hull surface*

using integrated fluid forces and moments. Conventional virtual tank model for displacement hull uses 2-DOF with incoming velocity & stationary domain. In contrast, for high-speed vessel and for ramping up velocity this approach can be impractical. Hence, 3-DOF approach is used here with surge motion along with free pitch and heave. The domain contains stationary water and overset domain moves in forward direction to depict the surge motion of the vessel.

It is also impractical to have very large background domain to capture the final state of the vessel, which can be of several lengths of the vessel. To have a reasonable size of the virtual tank domain, 1-DOF surge motion matching the motion of overset grid is applied on background domain as well. This approach will make the size of the computational domain reasonable and the overset grid will always remain in the center of the background domain.

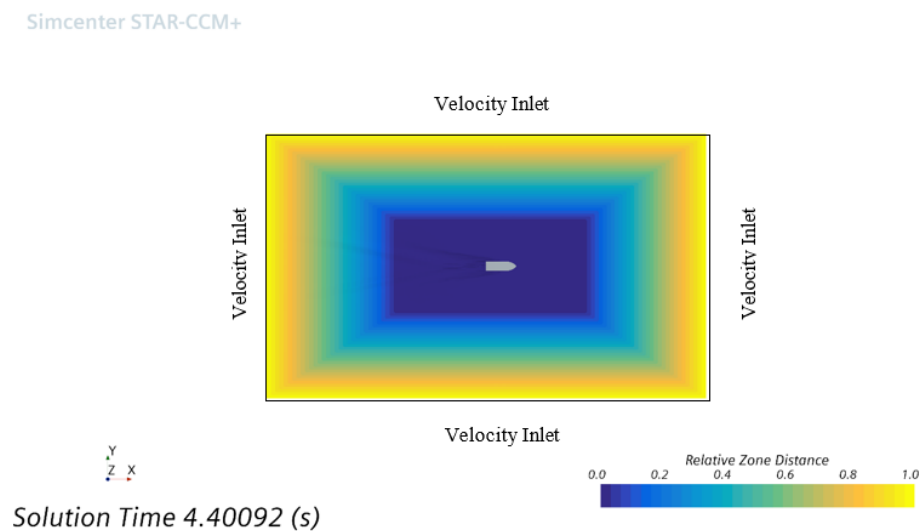


Figure 27: *Wave Forcing Zones and Boundary Conditions - Top View*

The imposed translation of background mesh uses wave forcing treatment, applied

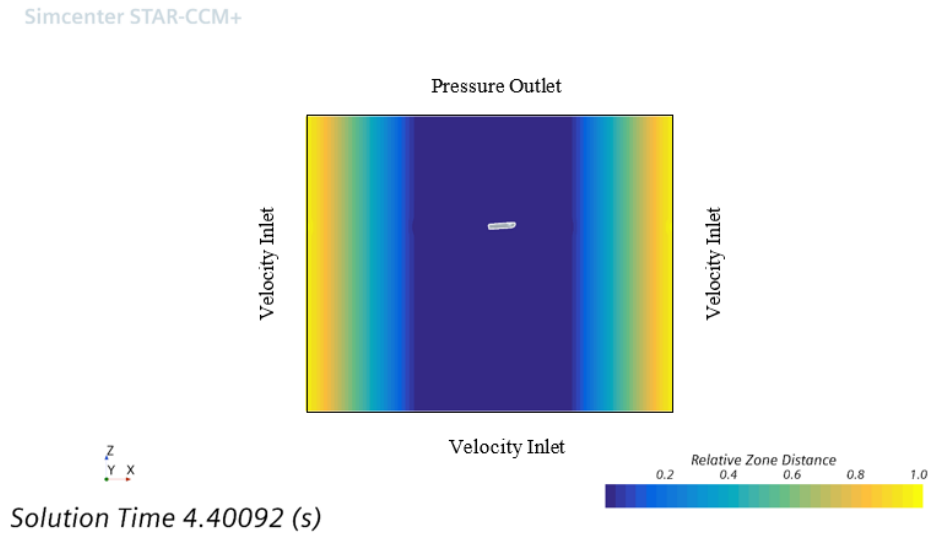


Figure 28: *Wave Forcing Zones and Boundary Conditions - Side View*

in the buffer layer near the vertical walls as shown in Figure 27 and 28. Velocity inlets with zero velocity are prescribed at the domain boundaries, while pressure boundary condition at the top of the domain ensures a hydrostatic applied gradient. No-slip boundary condition is utilized near the vessel boundaries, and symmetry along the y-section is used to reduce computational time. Forcing is achieved by an additional term on the right hand side of momentum equations. Brief numerical equations about it are presented in Appendix C.

$$q_\phi = -\gamma\rho(\phi - \phi^*) \quad (3.1)$$

Virtual Disk & Propeller Method

The significance of using body force propeller method to simulate the effect of propeller forces is highlighted in the previous section. The utilized DFBI method uses general planar carriage motion to accelerate the ship up to required speed. Further, RPMs and thrust forces are adjusted using employed equations and JAVA macros to match the vessel speed. Propeller thrust as well as propeller RPMs and consequent engine power are available at the disposal using propeller open water curves.

Eventhough, engine power is the main objective function to minimize in real conditions. By doing so, the effect of propeller working point and efficiency should also be considered in the optimization framework. To simplify the analysis, and to solely focus on the optimization of the hull shape, propeller thrust is taken as the objective function to be minimized.

3.3 Automated Software Connection

For any optimization studies, several designs have to be tested in order to reach the relatively better design. In practical aspects, it is essential to automate the optimization workflow and remove the need of human intervention. Previous two sections have developed the concepts behind making of parametric model in CAESES and the numerical set-up for CFD computations in STAR-CCM+. In this section, brief description about the automation procedure is introduced.

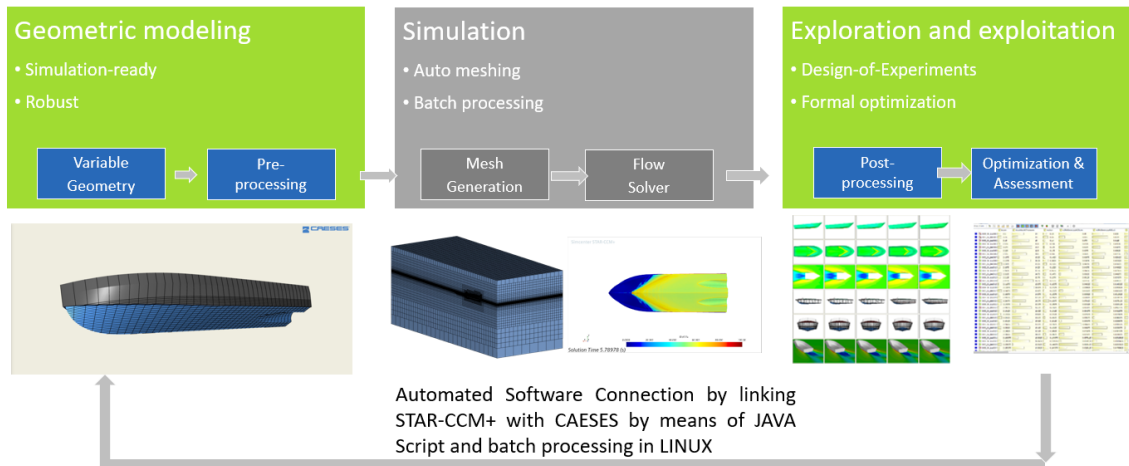


Figure 29: *Process Flow Diagram for SDD of Planing Hull*

The complete optimization frame work is given in Figure 29. JAVA macro's defines the connection between the two software. These macro's can be recorded in STAR-CCM+ and imported in CAESES, which gives the control to link the variables from the JAVA file to the optimization algorithm. The workflow also gives the command to adjust the previously defined macro by writing own JAVA scripts. By doing so, the need of redefining and re-recording macros is eliminated.

Moving forward, the complete set-up and connections for the optimization are transferred to the High-Performance Cluster accessed by LINUX. A bash script written in LINUX takes the name of the design optimization engine as the input. Then, it runs the optimization on cluster and moves back the simulation files in GUI for visualization of optimization runs. Figure 30 and 31 presents the tested several designs and their monitored convergence histories. It can be seen that most of the tested designs have shown good convergence plots. These plots are beneficial for post-processing, not only for graphical plots but also for geometry visualization. Pressure distribution highlighting the wetted surface area is also monitored for each design, as shown.

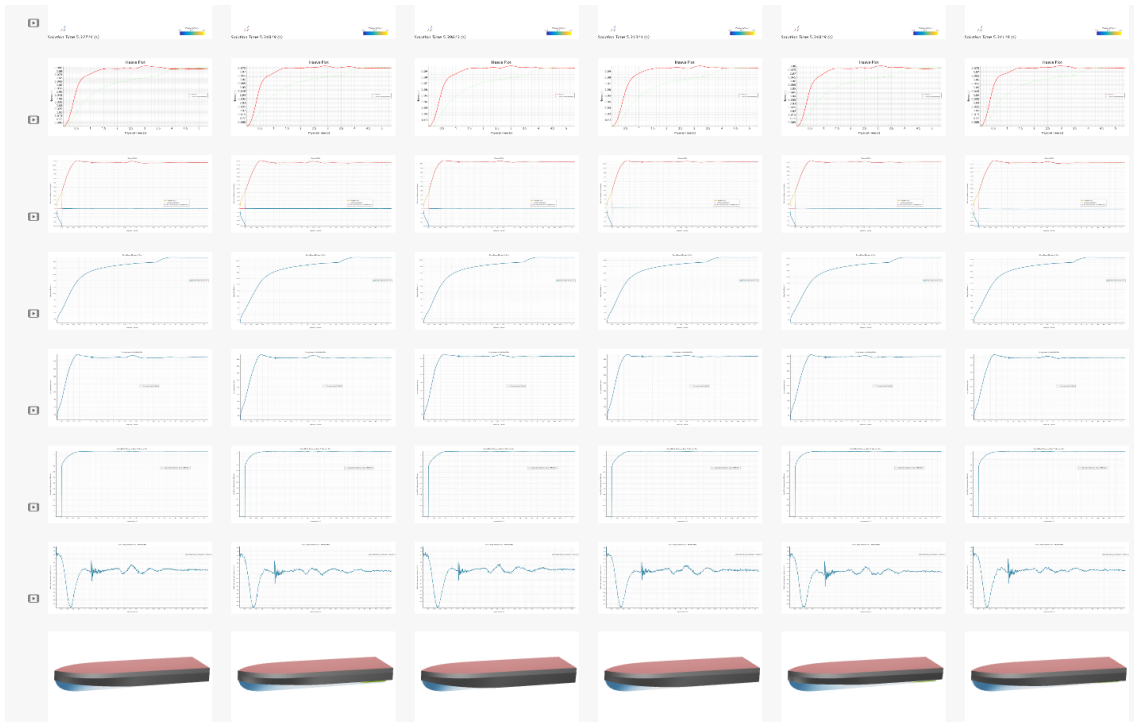


Figure 30: Automated Software Connection Convergence Histories

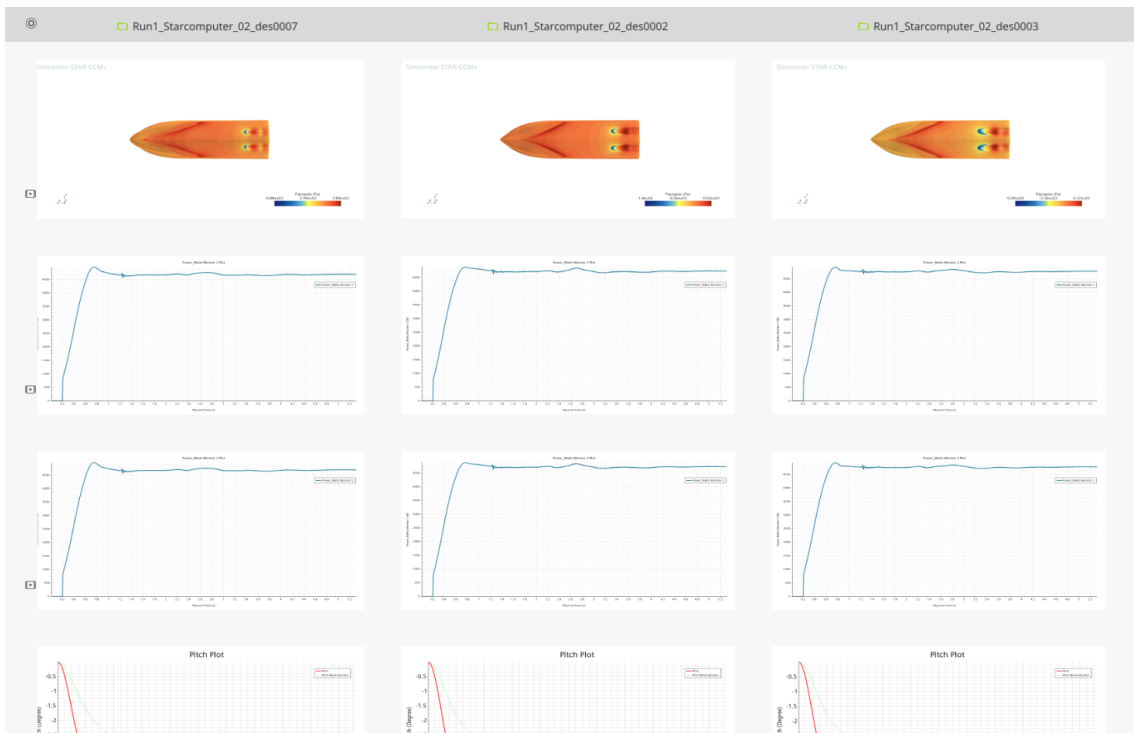


Figure 31: Automated Software Connection Convergence Histories Monitors

3.4 Speeding-up CFD Computations

While previously described techniques are utilized so that to have accurate prediction of objective function for optimization, with reduced computational resources. Few more steps to decrease the convergence instabilities and decreasing the time taken to achieve steady state values are presented here. To summarise, the methods enforced to speed-up CFD computations are given here.

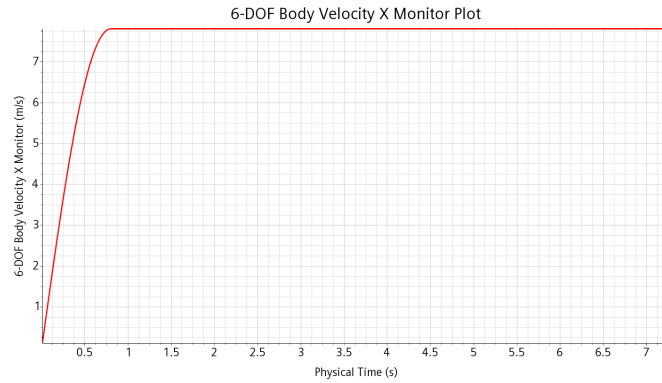
- Dynamic tight - overset grid with combination of adaptive mesh refinement and forcing zones, ensures faster convergence and relatively accurate predictions.
- Volume of Fluid (VOF) Slip-velocity method to remove artificial air beneath the hull, without using much finer grids.
- Use of Implicit Multi-Step time steps for faster convergence.
- Adaptive time-step is chosen to target courant number upto 5 for acceleration phase and less than 0.5 for the steady state final steps.
- Ramping up the velocity using a sinusoidal equation starting from rest position to smoothly reach design speed, with larger time steps.
- Artificially damping the motion of the vessel to reach steady state at lesser solution time.

Ramping up the velocity as defined previously, uses smooth transition and adaptation of dynamic body motions along with associated mesh motions. Hence, the velocity input to DFBI vessel is defined as a sinusoidal input reaching required speed as given in equation 3.2.

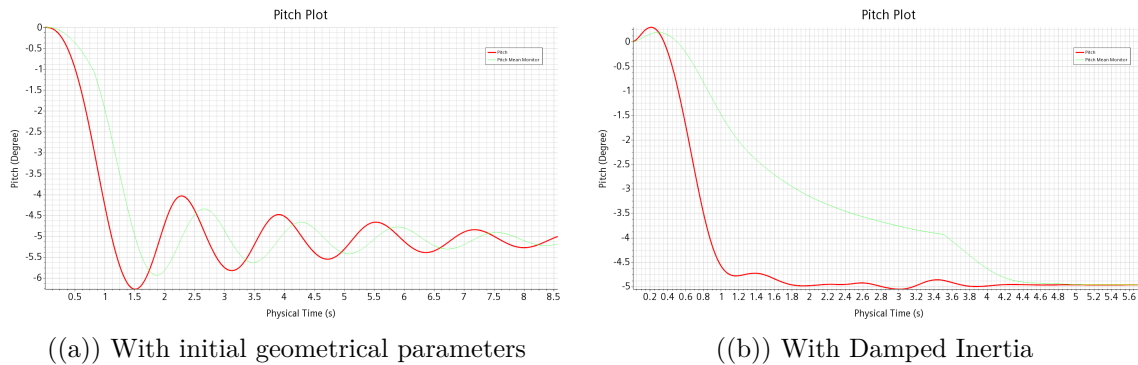
$$\text{If } t < T_r \quad V(t) = V_t \sin\left(\frac{\pi t}{2T_r}\right) \quad \text{Else } V(t) = V_t \quad (3.2)$$

This approach is effective in way to avoid large motions at the initial time steps and to avoid excessive pressure forces on the hull. T_r is the ramp up time and is set to have maximum acceleration of $1g$ (10 m/s). T_r value is 0.8s in this work, and design speed is 27.5 Knots full scale or $V(t) = 7.802 \text{ m/s}$ at the model scale. Figure 32 presents the input velocity for DFBI motion.

The use of ramp for the prescribed velocity of the body should be chosen with care. Steeper ramps can make the vessel reach equilibrium at much less T_r values, but it

Figure 32: *Velocity Plot to reach design speed*

can also impose larger acceleration gradients that needs to be avoided. In contrast, using high T_r value with much less acceleration can increase the computational time substantially. In this work, max acceleration of $1g$ is targeted to make a better compromise between the two. Despite that, as shown in left side of Figure 33 the acceleration forces which are directly linked with inertial properties of the body requires much higher time to dampen (in excess of 20 - 25s). To avoid larger computational time, the inertial forces are reduced by artificially reducing the inertial values of the vessel. As the requirement in given condition is to capture resistance and motion at the final-steady state conditions, dampening the inertia does not have any effect on the final solution as shown in right side of Figure 33.

Figure 33: *Pitch Plots with original and modified Inertia values*

3.5 Optimization Runs

In the end, the previously described automated connection with employed techniques for faster CFD Computations is used to perform optimization runs. A series of optimization strategies including, deterministic and stochastic modeling, design of exploration and exploitation, and Machine learning based surrogate models are uti-

lized to find a set of optimized designs. To better explain the optimization workflow, Figure 34 presents the flowchart used for optimization studies.

After testing initial baseline with CFD as well as tank tests, both of the computations have shown undesirable propeller and motion characteristics. Taking this into account, the first baseline was manually modified to have better rudder efficiency and dynamic motions. The modified geometry which is called New Baseline, now serves as the starting point of optimization and it has same principal dimensions as mentioned in Table 1 but with a change in draft and tunnel geometry.

Starting from this new baseline, the optimization runs are performed on full model with 18 design variables, as well as KLE model with 4 principal parameters. The optimization studies involves, Design of Experiment (SOBOL), Response Surface Optimization (DAKOTA), Tangent Search (T-search), Kriging and ANN based Surrogate models. By doing so, 7 best optimized designs are obtained and the quality of obtained designs against time taken to find them, are compared. The concept behind obtaining the new baseline, along with the results of each optimized design is presented and compared in the upcoming sections.

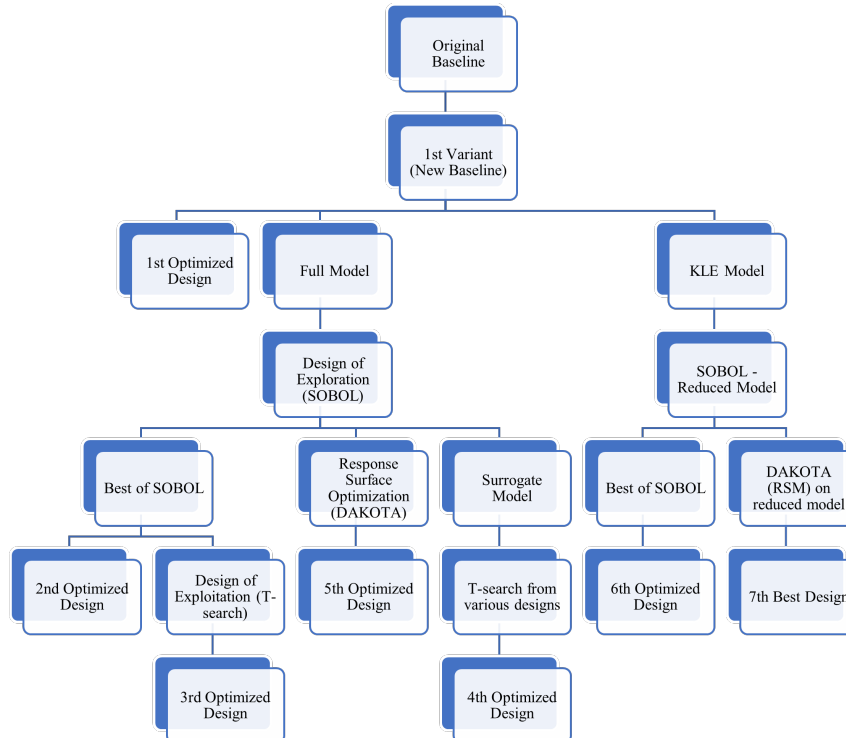


Figure 34: *Hierarchical View of Optimization Runs*

Chapter 4

Results and Discussion

Before starting for any optimization runs, it is essential to perform verification and validation analysis of CFD setup. The results presented here are verified by performing conventional grid convergence studies, along with quantification of grid uncertainties using Richardson Extrapolation Factor of Safety method (Xing and Stern 2010) . The results are then validated against the results of the tank tests available from Technische Universität Berlin (TU-Berlin).

First optimization studies involves conceptual changes to the tunnel geometry design after analyzing the results of both CFD and tank tests. Then, the new tunnel (updated baseline) geometry is tested again in the tank and validated by CFD results. Moving forward, the optimization is then performed on this new validated baseline. This section presents the results of previously mentioned studies. Furthermore, the results of subsequent optimization runs using the validated setup are also shown.

4.1 Verification and Validation

Verification and validations are two important steps for any numerical simulation. Briefly describing, verification refers to determining the numerical accuracy of the predicted results by varying grid sizes. Validation on the other hand is the step where the results of numerical code is compared with real-life experimental test data. These two steps are essential to quantify and measure any numerical uncertainty present in the code, and to compare the validity of numerical model with real life examples.

In this study, verification and validation are performed with some appendages to depict the experimental study. Also, this detailed analysis is focused on Resistance Tests to compare drag and motions. The study is then extended to validate one particular case of self-propulsion and to use it for the optimization studies.

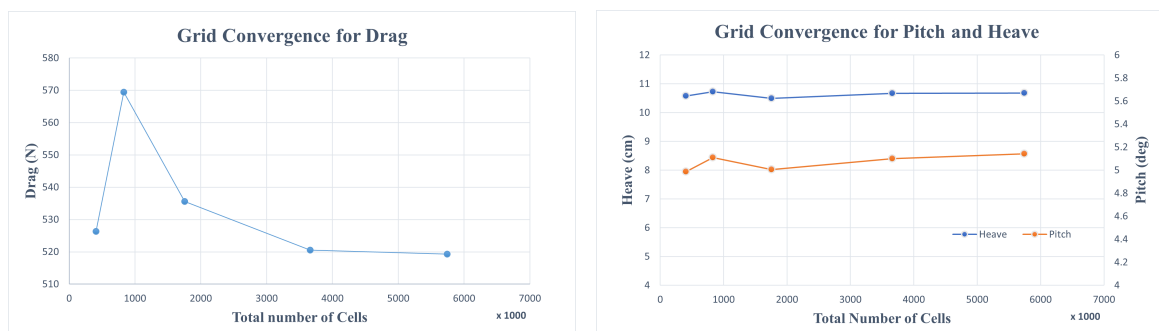
4.1.1 Grid Convergence Studies

To test grid dependence, 5 different mesh sizes with different background and overset grids are used. Coarsen Factor (R) is a parameter defining the grid sizes such that the grid sizes are varied uniformly and same ratio of cells in background and overset domain is guaranteed. This is important for the reason of data transfer between the two domains, and it can directly affect the solution accuracy.

Background and overset meshes are varied according to R values as, $L/5R$ for background mesh and $L/100R$ for overset mesh. Where, L corresponds to length of the vessel $L_{pp} = 3.364m$ in this case. R value starts from $1/2$ and it increases by a factor of $\sqrt{2}$ with finer grid sizes. Details about the grid convergence studies is given in Table 2.

Figure 35 highlights the convergence plots for Drag force and for dynamic motions of sinkage and trim angles. It can be seen from the figure that drag force converges after Mesh 3. For pitch and heave, the utilized grid sizes does not affect the values drastically. The relative percentage errors for Mesh 4 and Mesh 5 are less than 2 % for Drag and motion values.

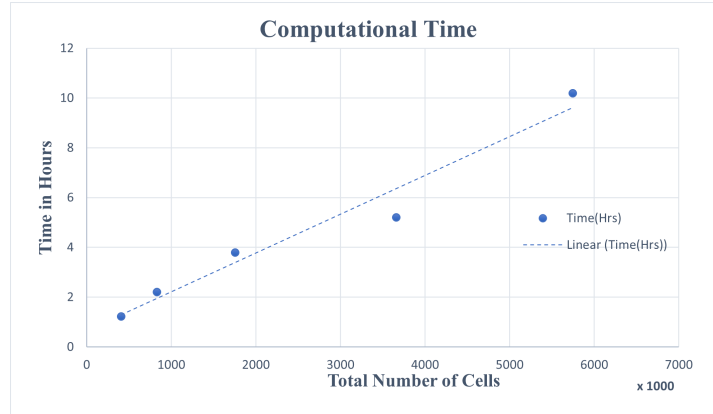
To reach a good compromise, other than accuracy of the solution the computational time should also be taken into account. Figure 36 shows the time taken for each mesh size until convergence. Mentioned time are for a HPC Cluster with 40 cores and 90 GBs of RAM. Computational time between Mesh 4 and Mesh 5 is almost double, while very less improvement in accuracy of solution is observed. Based on these analysis, Mesh 4 with grid size of $3.6M$ and computational time of almost 5 Hrs is adapted for validation purpose.



((a)) For Drag Force

((b)) For Pitch and Heave

Figure 35: *Grid Convergence Studies for motions and forces*

Figure 36: *Computational Time of different Grids*Table 2: *Grid Convergence Studies Parameters*

Name	Base Size		Total Cells	Time Hrs	Coarsen Factor	Heave cm	Pitch deg	Drag N
	Background m	Overset m						
Mesh 1	1.35	0.065	408676	1.22	0.5	10.581	4.9867	526.36
Mesh 2	0.95	0.05	831152	2.21	0.7071	10.727	5.10946	569.42
Mesh 3	0.67	0.035	1755600	3.79	1	10.4975	5.0044	535.572
Mesh 4	0.48	0.025	3661000	5.2	1.4142	10.667	5.1003	520.557
Mesh 5	0.4	0.02	5745000	10.2	2	10.679	5.143	519.271

4.1.2 Quantification of Grid Uncertainties

For numerical solutions such as CFD, quantifying the uncertainties in grids are of particular interests. The idea is to find the function value as the grid size approaches to zero. Theoretically, this value is called exact value and it should be equal to the real value of the physical system. As it is not possible to have grid size zero practically, there are some methods to quantify the percentage difference with the finest acquired grid and its exact value, determined theoretically.

Conventional method of quantifying the uncertainties are Grid Convergence Index (GCI), Richardson Extrapolation and many others. In Table 3, grid uncertainties of Drag, Pitch and Heave are highlighted using Richardson Extrapolation Factor of Safety method (called as FS) and GCI.

Table 3: *Grid Uncertainty Quantification Values*

# of Cells	R	Drag (N)	Pitch (Deg)	Heave (cm)
1.76E+06	1	535.57	5	10.5
3.66E+06	1.4142	520.56	5.1	10.67
5.75E+06	2	519.27	5.14	10.68
Uncertainty_FS	%	0.753	4.647	0.31
Uncertainty_GCI	%	0.029	2.867	0.011

Comparing both of these quantification methods, GCI is less conservative as compared to FS method. Similar findings are observed in other papers. It should be taken into account that these uncertainties does not necessarily quantify the percentage difference with the experimental values. But, can give a good indication of grid convergence. Higher uncertainties in pitch can be justified due to smaller absolute differences. Because the values are smaller, the percentage difference scales up. Figure 37 and 38 shows the evolution of drag, pitch and heave as the grid size approaches to zero. S_c corresponds to the exact value of the numerical solution, calculated theoretically.

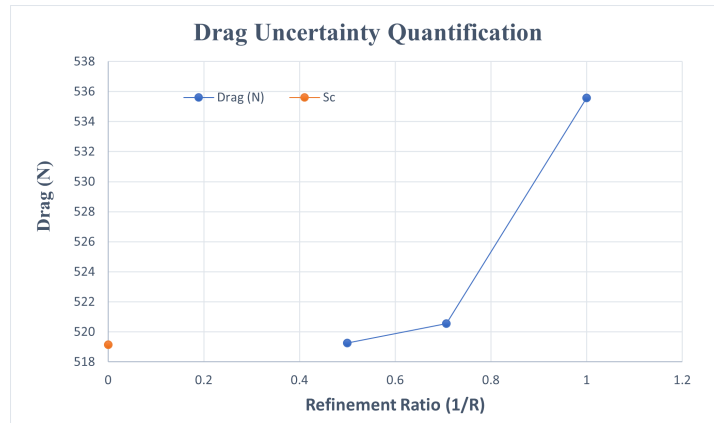


Figure 37: *Uncertainty Quantification for Drag Force*

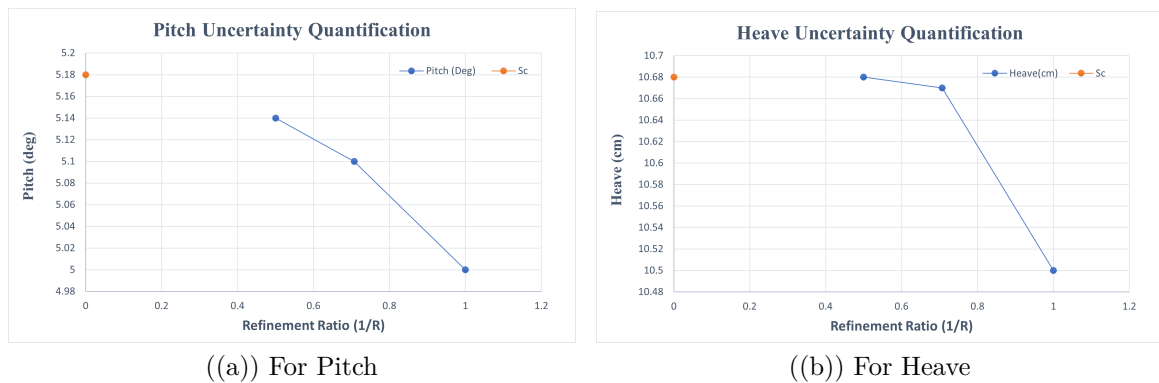


Figure 38: *Uncertainty Quantification for Pitch and Heave*

4.1.3 Validation Studies

After the appropriate selection of the mesh size and quantification of uncertainty associated with it, the numerical model is then validated against the experimental data available. Resistance tests performed in a tank tests is validated by a virtual tank test simulated in STAR-CCM+ computations. The observed results suggested a good comparison between the two setups.

Table 4: Validation at Design Speed

Fr	V(knots)		Error estimation		
	Full Scale	Model Scale	Drag (%)	Heave (m)	Pitch (deg)
1.3581	27.5	15.18	0.2684	0.0114	0.88

Figure 39 and 40 below shows the comparison of numerical and experimental results. For comparison, simulations are carried out with different velocities ranging from Froude number 0.8 to 1.45. Resistance forces have good comparison with percentage difference of less than 1%. For trim and heave comparison, it is feasible to compare the absolute difference because of smaller values. Comparison of pitch motion shows the maximum deviation of 0.9 degree. For sinkage motion, the experimental data was only available for the design speed and shows difference of 1cm.

Focusing on optimization, it is desirable to optimize the hull design at the design speed of 27.5 knots. Table 4 shows the validation studies at design speed. Taking into account the grid uncertainties defined previously and assuming measurement uncertainties of 5-8 % the simulated CFD setup is considered to be validated.

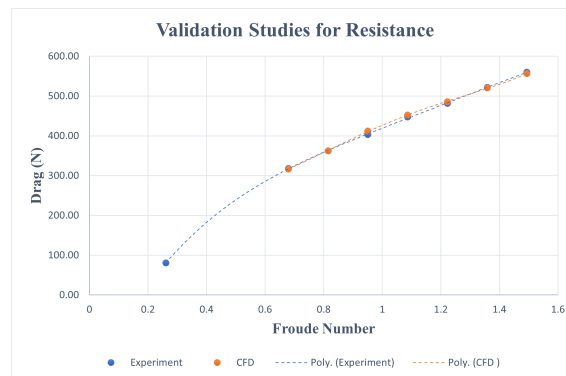
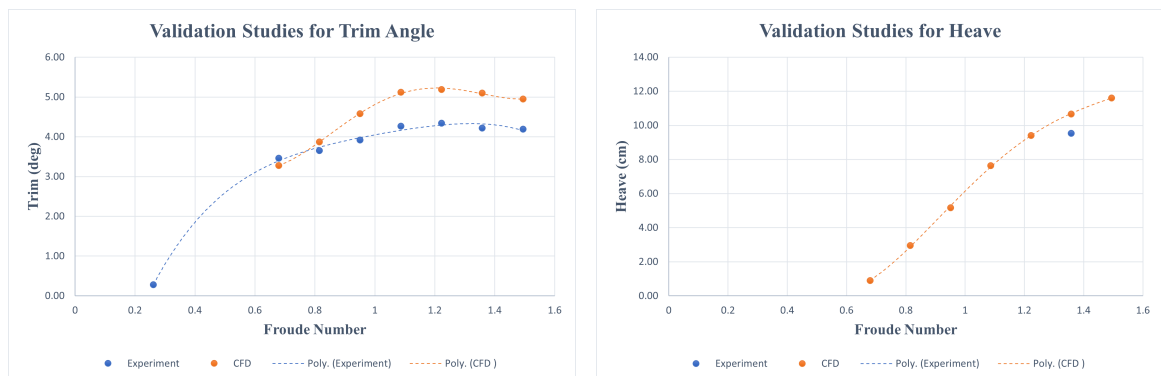


Figure 39: Validation for Drag Force against Experiments



((a)) For Pitch

((b)) For Heave

Figure 40: Validation for Pitch and Heave against Experiments

4.2 First Optimization Study

For the first optimization studies, the initial baseline is analyzed and conceptual changes are made in the tunnel geometry from the outcome of the tank tests and simulations. It has been observed that the initial baseline has cross-flow around the wake and higher wave elevation behind the transom. This phenomenon also resulted in poor rudder efficiency, highlighted from tank tests results.

In order to overcome this issue before the optimization phase, tunnel parametric model is adapted with new parameters. These parameters are taken in order to avoid the cross-flow, and have relatively lower wave elevation behind the transom. Proceeding with this concept in principal, has also reduced the pressure drag or wave making resistance of the vessel. Parametric models of two tunnel geometries is given in Figure 41. Visual comparison of the free surface elevation for both of these geometries is shown in Figure 42 and 43.

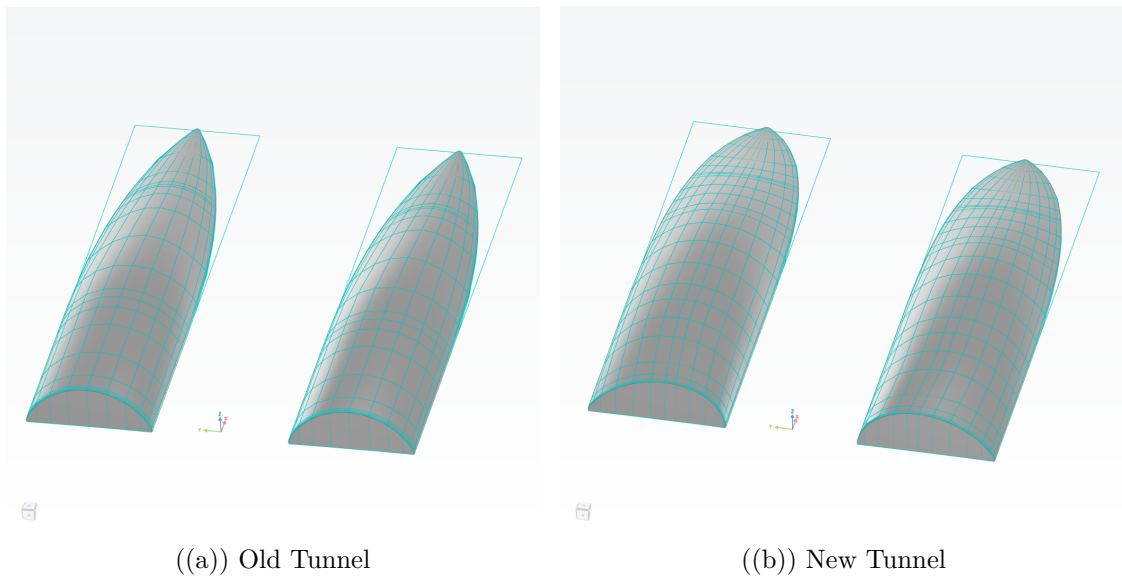


Figure 41: *Old and New Tunnels Geometries*

While this new geometry provides smoother flow around wake, and better rudder efficiency in tank tests. The results of the tank tests have shown similar drag values for this new geometry. In order to analyze it, CFD computations of same setup are undertaken and components of pressure and shear drag are computed separately. As shown in Table 5, the pressure drag has been reduced as evident by relatively smoother flow. In contrast, the gain acquired by decrease in pressure drag is negated by the significant increase in the shear drag component.

The subsequent increase in the shear drag is due to the increase in wetted surface

area for the new geometry. Figure 44 compares the pressure distribution of the two designs. It can be observed that the new geometry is in the semi-planing regime with larger wetted surface area. The reason behind this is not having enough lift force to lift the vessel out of the water, and therefore relatively lesser trim and rise values.

The results of this study, highlights the importance of clearly defining the objective function. Some possible objective functions can be, to minimize the total drag or its individual components. Maximization of lift force can also be taken as an objective function for the optimization.

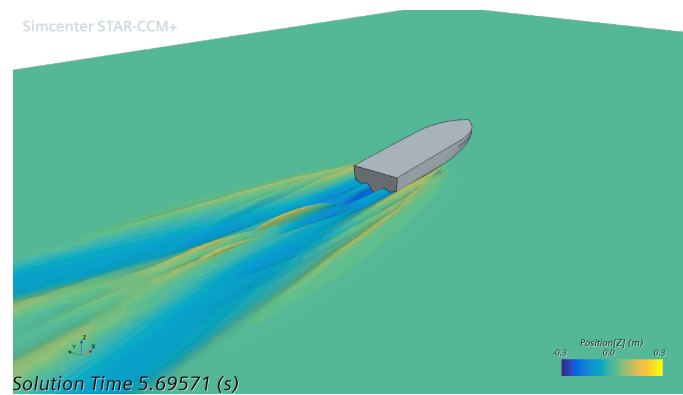


Figure 42: *Free Surface around wake for Old Tunnel Geometry*

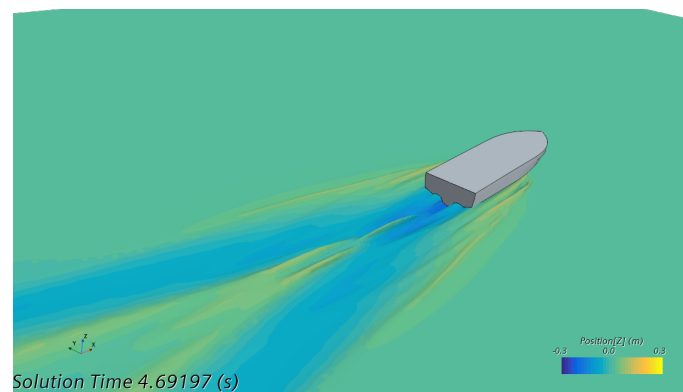


Figure 43: *Free Surface around wake for New Tunnel Geometry*

Table 5: *Comparison of the old and new tunnel*

	LCG (m)	XCB (m)	Resistance (N)	Trim (Deg)	Heave (cm)	Pressure Drag (N)	Shear Drag (N)
Old	1.504	1.4681	521.52	5.09	10.06	311.68	209.84
New	1.504	1.4681	520.62	2.98	6.96	263.38	257.24

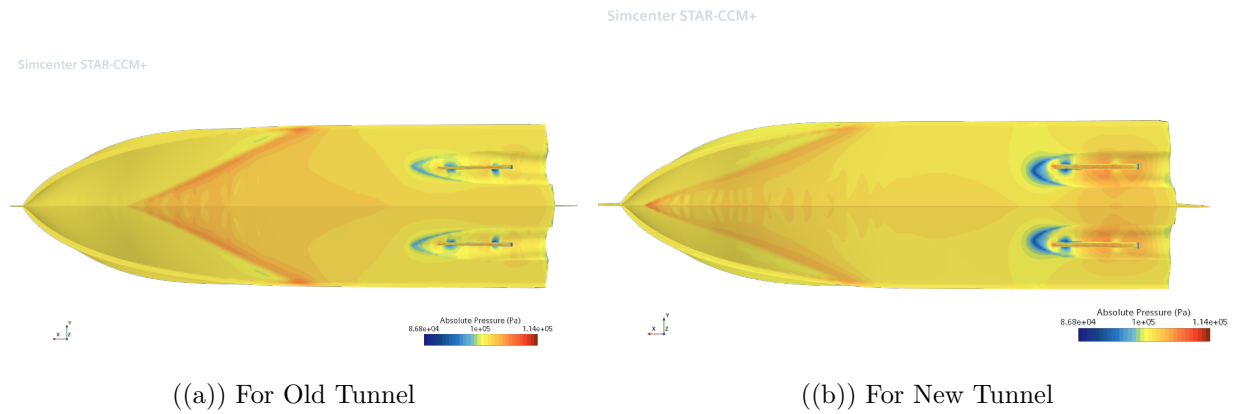


Figure 44: *Pressure Distribution for old and new tunnel geometries*

Validation for Self Propulsion Tests

Resistance tests simulations are extended to incorporate the effect of propeller forces, by performing self-propulsion tests. The importance of dynamic trim and rise in the context of optimization is discussed previously. Furthermore, the presence of propeller forces in the momentum equation can directly effects the running attitude and corresponding resistance of the vessel.

Taking this into account, propeller thrust is taken as objective function for optimization by creating a virtual disk model. Before proceeding with the optimization, validation studies were performed at design speed. Table 6 presents the experimental and CFD results, which shows a promising comparison.

Table 6: *Validation with Propeller Method*

Property	Experiment	CFD	Units
Thrust	532.08	520.4	N
RPMs	2285.7	2280.29	/s
Torque	25.65	24.44	N.m
Power / motor	3.0698	2.9180	kW / motor
Pitch	3.44	3.67	deg
Heave	7.98	7.92	cm

4.3 Numerical Model Adaptation

Speeding-up of an optimization task does not only come from faster and effective optimization methods. Instead, simplification of the numerical model using applied assumptions also plays an important role. For example, using relatively coarser grid or removing appendages that are not part of optimization studies. After validation

of numerical setup the target is to find an optimized design with respect to baseline. In this case, it is convenient to simplify the whole system by using these assumptions and compare the relative percentage difference against the baseline of a simplified system. Afterwards, few optimized designs obtained using a simplified and much faster system can be transformed back to appended model and the actual percentage improvements are checked by using finer grid sizes.

4.3.1 LCG Sensitivity Analysis

Before moving with the simplification steps, the target was to improve the planing performance of the new baseline. This consideration comes after looking at the pressure distribution of new baseline as in Figure 44, which represents that the vessel is in semi-planing regime. To improve the planing characteristics, a shift of longitudinal center of gravity (LCG) towards aft is proposed.

Planing vessels are very sensitive to LCG positions as studied by different authors in literature. The proposed shift in LCG position is also backed by the fact that at the hydro-static position, the vessel has a -0.22 degree trim angle which is not desirable. Negative trim angle is due to the position of center of buoyancy (CB) which is few percentage aft from current LCG position.

Table 7: *LCG Sensitivity Analysis*

LCG (m)	Resistance (N)	Trim (Deg)	Heave (cm)	Pressure Drag (N)	Shear Drag (N)	Static Trim (deg)
1.504	520.62	2.98	6.96	263.38	257.24	-0.22
1.468	515.01	3.20	7.57	263.29	251.72	0.00
1.454	511.72	3.26	7.74	261.42	250.3	0.06
1.404	501.5	3.43	8.34	257.66	243.84	0.23
1.354	491.8	3.63	8.96	255.30	236.50	0.43
1.254	478.62	4.02	10.28	258.18	220.44	0.82
1.154	472.5	4.42	11.74	267.02	205.48	1.22
1.054	465.18	4.82	13.34	277.92	187.26	1.62

To quantify the effect of LCG shift on vessel performance as well as on drag components, LCG sensitivity analysis as given in Table 7 is carried out. LCG is shifted from its original position of 1.504 m to 5 cm aft in each iteration. The results of dynamic motions as well as resistance is presented. Static trim angle is -0.22 deg for the initial LCG position and 0 deg of static trim angle is observed for LCG of 1.468 m, as this is also the position of center of buoyancy. When, LCG and CB are in the same vertical plane there are no added momentum to produce static trim at the hydro-static position of the vessel.

Plots of above given table is presented in Figure 45. On the left hand side, it is highlighted that shifting the LCG position towards aft in the given setup improves the performance of the vessel. This is due to the subsequent reduction in shear drag component due to the decrease in wetted surface area, and increase in pitch and heave motions. It is also interesting to see each component on drag individually, as in the right hand side. Individual component of drag forces behaves differently as we shift LCG significantly towards aft of the vessel. Increase in the pressure drag occurs due to increase in the wave making resistance of the vessel, backed by larger trim angle. While, the decrease in the frictional drag occurs due to the decrease in wetted surface area of the vessel.

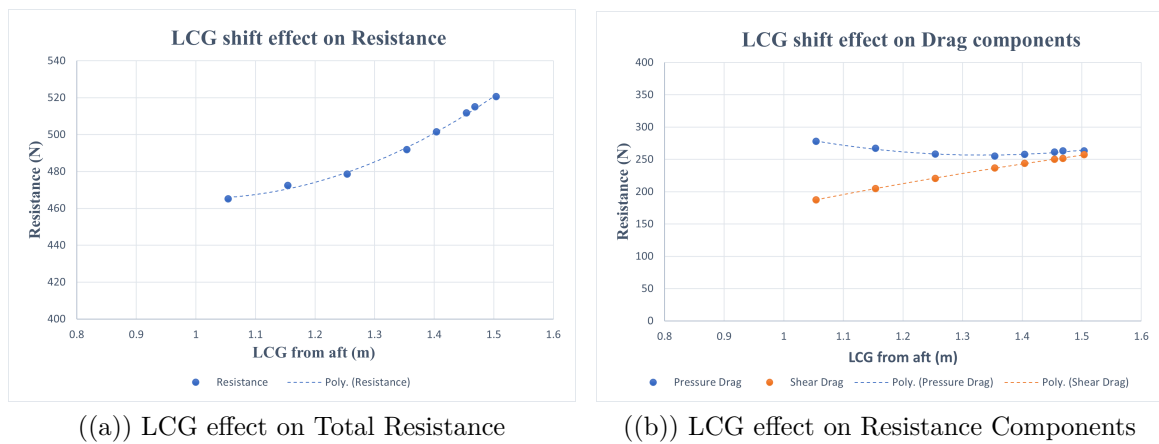


Figure 45: *LCG Sensitivity Analysis*

This study gives important aspects that should be taken into account while performing optimization for a planing craft. In the light of this, the proposed value of LCG is 1.354 m that is, 15 cm shift from its original position. In full scale, the shift in LCG position is 50 cm and calculated to have static trim angle of around 0.45 degrees. The shift in LCG improves the performance of the vessel by around 4% as given in Table 7.

4.3.2 Effect of Appendages

Moving forward with the model simplification tasks, this section presents the optimization studies carried out for 5 designs with and without appendages. This is done to check the influence of the appendages on the vessel performance. 5 designs are generated using Design of Experiment (SOBOL) by varying different design parameters. The results of these designs with and without appendages are given in Table 8, the table is arranged chronologically with respect to drag values.

Absolute differences for forces and motion values are also presented in this table.

Table 8: *Effect of Appendages on Designs Performance*

Designs	With Appendages			Without Appendages			Absolute Difference		
	Drag (N)	Heave (cm)	Pitch (Deg)	Drag (N)	Heave (cm)	Pitch (deg)	Drag (N)	Heave (cm)	Pitch (Deg)
Des0003	534.27	7.0842	-2.99	476.08	5.8328	-2.77	58.19	1.25	-0.22
Baseline	532.33	6.9755	-2.89	477.64	5.8468	-2.80	54.68	1.13	-0.10
Des0002	537.72	6.9682	-2.90	484.81	5.8924	-2.79	52.90	1.08	-0.11
Des0000	551.98	6.2163	-2.36	500.85	5.2414	-2.23	51.13	0.97	-0.13
Des0001	576.55	5.6768	-1.90	538.55	4.6621	-1.71	38.00	1.01	-0.19

Based on the observations, the effects of appendages can be seen to have an added resistance effect. This added resistance varies from 30 to 50 N for each design, while averaging around 50 N . Heave and pitch values also have same effects of appendages, increase in heave by around 1 cm and pitch angle is reduced by 0.15 degrees. In contrast, taking into account appendages into simulations also requires resolving the appendages with finer grid sizes. Simulation time with appendages is 5 hours (Mesh 4) while without appendages is 3.5 hours (Mesh 3). Taking this into account, the simulation studies are carried out without appendages and with smaller simulation time. Ranking of designs for the simulated model with and without appendages, remains same except for Des0003 and Baseline which are within numerical uncertainty of 1 %.

4.3.3 Effect of Mesh Refinement

Similar studies are carried out for the effect of mesh size on the designs performance. Mesh 4 from the convergence studies is compared with Mesh 2, solution values along with absolute differences are presented in Table 9. The obtained results highlights the same findings as for the effect of appendages. In contrary, using Mesh 2 decreases the computational time to 2.5 Hrs from 5 Hrs. Absolute differences shows that both of these meshes does not significantly alters the motion values, only the drag values changes by 5 to 10 N .

Table 9: *Effect of Mesh Size on Designs Performance*

Designs	Mesh 2			Mesh 4			Absolute Difference		
	Drag (N)	Heave (cm)	Pitch (Deg)	Drag (N)	Heave (cm)	Pitch (deg)	Drag (N)	Heave (cm)	Pitch (Deg)
Des0001	444.49	6.8078	3.31	434.25	6.8590	3.34	10.24	-0.05	-0.03
Des0003	446.40	6.6714	3.32	438.12	6.7170	3.35	8.28	-0.05	-0.03
Des0000	451.22	5.7720	3.22	445.34	5.8646	3.30	5.88	-0.09	-0.07
Des0002	468.86	4.5263	3.10	462.01	4.6536	3.17	6.85	-0.13	-0.07
Des0004	477.78	2.8527	2.94	468.38	3.1885	3.08	9.40	-0.34	-0.15

4.4 Optimization Runs

For the optimization runs, various deterministic and stochastic methods are tested and compared. Following mentioned points highlights the brief summary of the optimization studies.

- Propeller thrust is the objective function for optimization while using body force propeller method in CFD simulations.
- Initial baseline is modified with new tunnel geometry, the new geometry is termed as 'Baseline' for the context of optimization runs.
- For the new geometry shifting LCG 15cm aft, improves the performance by 4-5 %. Hence, before starting the conventional optimization runs around 5 % thrust deduction is already achieved.
- In the following sections, the already improved design with shifted LCG and new geometry is termed as 'Baseline' and serves as the starting point of optimization runs.
- Simplifications for the optimization runs are employed, this involves using coarser grid and removing the appendages.
- The final set of best designs found out using different optimization techniques, are back transformed to actual model with appendages and with finer grid size.
- Comparison for the total thrust reduction achieved by using different optimization strategies against the time taken is shown.

4.4.1 Design of Experiment (SOBOL)

SOBOL is a method of Design of Experiment employed for exploration of the design space. It is a good indicator of analyzing the correlations between the objective function and different design variables. For the SOBOL analysis, 100 designs are generated and computed with automated simulations setup. Figures 46 presents some of the correlations for some design variables. The color of the plots highlights the linear correlations and its strength. With red or orange shows increasing plots of direct relationship and blue plot showing decreasing plots or inverse relationship.

It is also interested to see the effect of pitch, heave and drag values on the propeller thrust. As expected from previous study, drag increases linearly with the increase in thrust value. Also, higher pitch angles and rise is associated with lower thrust values. More correlation plots are attached in Appendix E.

4.4.2 Deterministic Tangent Search (T-search)

While design of experiment is useful in analyzing the sophistication of the baseline, it can also produce some relatively better designs as compared to initial geometry. These designs can be termed as optimized designs from DOE analysis. Furthermore, they can serve as a good starting point (initial condition) for the deterministic optimization search. In this study, the focus is based on T-search (Tangent search) method of deterministic (local) optimization.

The working of T-search model is based on the pattern search. It is a gradient free optimization method. While staying in the feasible domain, it searches for the pattern towards the nearest minimum of the function. The pattern search always remains within the feasible domain (upper and lower limits of design variables). If at some iteration it goes into the infeasible domain it returns to the currently best or last design. The next design is searched along the tangent of the inequality constraints. The pattern search although does not include computing gradients, but it is based on developing patterns by changing each design variable and analyzing their influence on the objective function. After a pattern is developed, much larger step in the proposed direction is undertaken to reach the best possible design.

This method is useful for finding local optimum. Nevertheless, it involves perturbations of each design variable before finding a pattern. This leads to testing several designs based on number of design variables. Figure 48 presents the T-search carried out starting from design number 15 of the SOBOL optimization run. It involves 12 design variables out of 18 design variables tested originally. 6 design variables were removed to reduce the computational time of T-search, and by analyzing the correlation plots described previously. That is, the variables with little to no correlations on the computed thrust were removed for T-search.

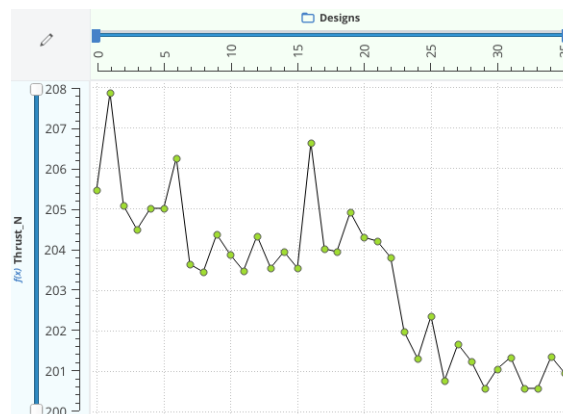


Figure 48: *Deterministic Optimization - Tsearch from best design*

The T-search started from Des0015 of SOBOL which is 5% improved with respect to the baseline, reaches the stopping criteria of maximum number of CFD iterations. Figure 48, it can be seen that the perturbations of design variables is carried out until 22th design iteration. After that, much larger step in the optimum direction is undertaken. The final design of the T-search is 2.3 % better than its starting point, and 8.3% better than the baseline of optimization start.

4.4.3 Surrogate Modeling

One of the potential task of this thesis was to explore the Machine Learning and AI-based optimization strategies, also called as Surrogate Models. The surrogate models uses the input data to train a model and make prediction of the new values. In this context, two types of Machine Learning models are used that includes Kriging and Artificial Neural Networks.

The input data for training is taken from the DOE results. The designs are distributed uniformly around the design space using SOBOL algorithm. Hence, this data serves as a good training set for the model. The quality of the generated model is often represented by its Coefficient of Performance (CoP) value. This value is calculated by training the model with a larger portion of the data set while comparing the predicted values with the remaining, but smaller portion of the data set. CoP values of around 1 is desirable ideally, but most of the ML models have been found to perform well with 95% performance or 0.95 CoP value.

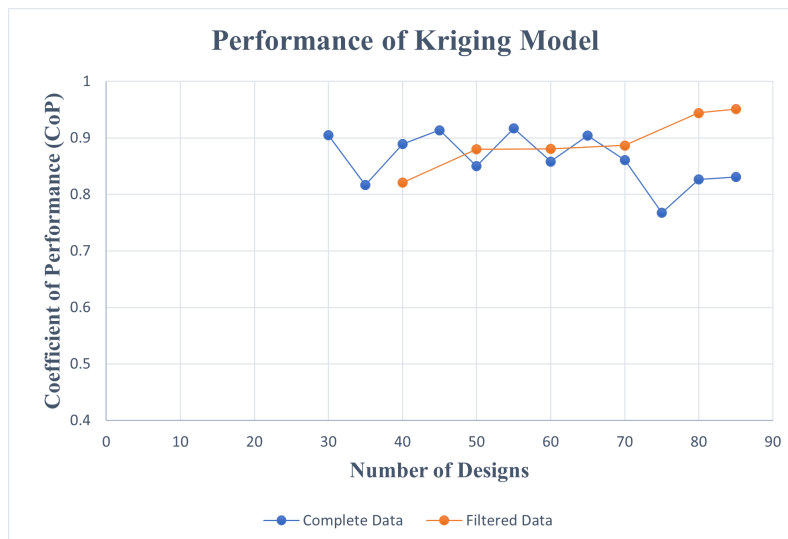


Figure 49: Performance of Machine Learning Model - Data Filtering

As in any regression analysis there can be some outliers, which should be removed in order to have better R^2 value. The same is true for sophisticated Machine learning

based models, Figure 49 presents the plots of CoP value of Kriging model with complete data set taken from SOBOL runs, and with filtered data after removing outliers. The outliers from the data is removed by writing a feature in CAESES that iteratively takes a portion of the data set by increasing sample size. If the performance is reduced by inserting a certain set of data (say designs 50-55), the function then calculates the effect of each of these designs on CoP value. Hence, removing the designs which are not well fitted with the Machine Learning model.

Table 10: *Kriging and Artificial Neural Network (ANN) Performance - Filtered Data*

# of Variants	CoP Value		Function Value	
	Kriging	ANN	Kriging	ANN
40	0.8212	0.8034	218.42	219.5
50	0.8796	0.7902	218.42	220.39
60	0.8809	0.9398	218.42	214.13
70	0.8867	0.9095	218.42	217.56
80	0.9446	0.8014	218.42	220.95

The approach used for data filtration is robust but not very efficient for larger data set. In this context, as the number of designs were limited to 100 it was feasible to use this method. For larger data sets, there are python libraries and functions that are being vastly used for data filtration. Table 10 presents the filtered data and highlights the performance of each ML model with the increase in the number of variants.

From this table, it can also be seen that the performance of kriging model improves with the increasing sample size. In contrast, ANN performance as well as the predicted function value for the baseline varies significantly. This is due to different working principle of each of them as explained in earlier sections. Everytime the model is generated back from scratch, ANN shows slightly different values while Kriging always predicts the same values for the given data set.

T-search based on Surrogate Model

After training the data set and having formed a good working Machine learning model, optimization is carried out using this model. For the optimization, Kriging based model is trained with around 90 design variants having filtered data and CoP value of around 0.95 or 95 %. Figure 50 represents the results of the T-search carried out using this model. To better visualize and make a comparison, the results of T-search starting from Des0015 using Kriging model is plotted with previous results. This includes the results of the initial SOBOL run, along with the T-search from Des0015 carried out using CFD as previously shown in Figure 48.

As compared to its CFD counterpart, the T-search based on Kriging model is relatively faster and hundreds of designs can be computed in few minutes. Therefore, the maximum number of evaluations for this model has been increased to 100 iterations. This gives the optimizer more time to find various optimums. One of the interesting feature highlighted in Figure 50 is the local plateau or minima found in between 40-50 iterations. This minima is found out by both T-search, using CFD and Kriging model. Variation of around 1 % is acceptable considering the CoP value of the ML model. In comparison, CFD computations uses much larger time to converge to the same design havig 8 - 9 % improvement against the baseline. If the simulations are allowed to run more for CFD computations, the proposed T-search is expected to find the same minima in 100 iterations. But, at the expense of several hours of computations.

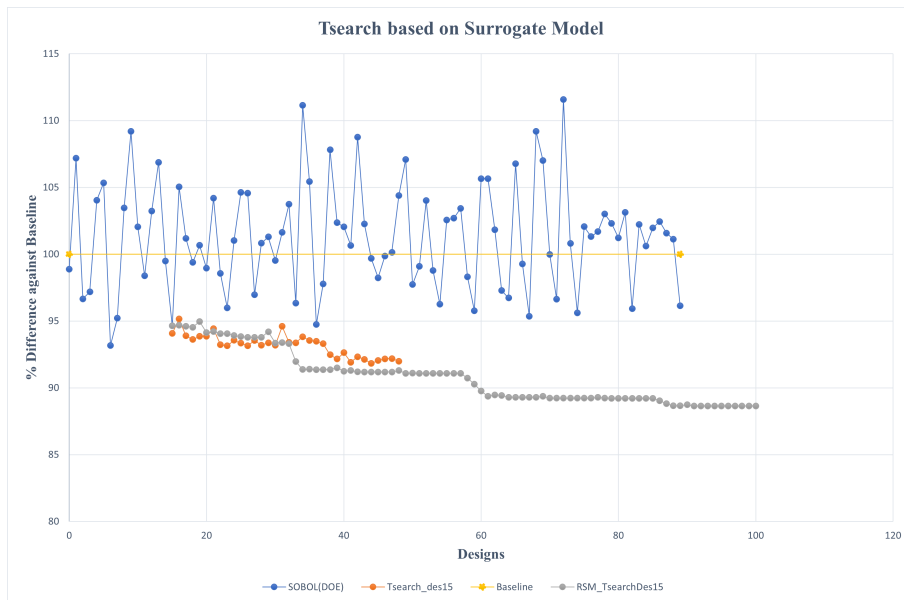


Figure 50: *Surrogate based Tsearch - Comparison*

Response Surface Optimization

Response Surface Optimization is another optimization genetic algorithm, it works similar to previously described Machine learning model. The difference being that it uses DAKOTA open-source libraries and creates a response surface for the optimization. Then, at the second step the genetic algorithm is run on the response surface model to find the global optimum of the initial surrogate model.

The data to train the response surface model can either be an input data, as in this case SOBOLO. If the data is not provided, the optimizer will create a design pool with minimum number of designs required for generating the model (which is equal to 5 x Number of Design Variables). If the data set is not provided, design pool

uses Latin-Hypercube Sampling (LHS) instead of SOBOL algorithm. LHS is also another type of DOE tool works differently than SOBOL, but for same purpose of exploring design space.

This work uses Response Surface Optimization with the data set previously generated with SOBOL. As an output, a new variant is created which has 11 % improvement against the baseline. The output result is also backed by running a CFD simulation by the algorithm itself. This newly created variant lies on the same location as the T-search from Kriging model between 60 to 90 iterations. To have a better comparison, Figure 51 presents the results of DAKOTA in comparison to previous optimization methods.

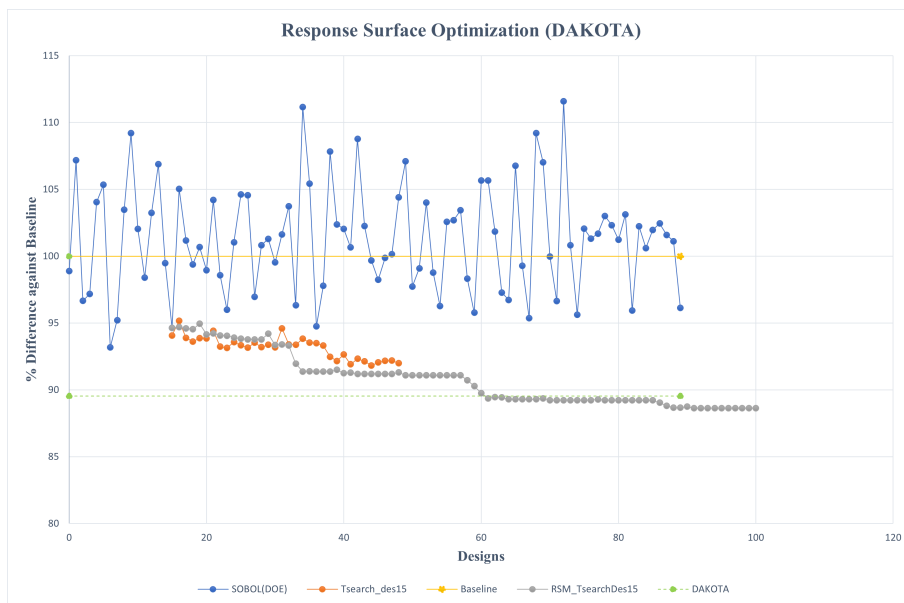


Figure 51: *Response Surface Optimization (DAKOTA)- Comparison*

4.4.4 KLE based Optimization

Another idea of decreasing the optimization time is to reduce the parametric dimensional space. As described previously, deterministic optimization strategies such as T-search uses several design iterations. These design iterations are the function of number of design variables. In this work, special form of Principal Component Analysis KLE is carried out to decrease the design space.

Table 11 presents the captured variance resulting from the PCA Analysis. 2500 samples are generated to train the PCA model, with 10000 points to resolve the CAD for each design. Presented results indicates the captured variance with each principal parameter. Three different columns shows the PCA analysis carried out for hull and tunnel geometry separately, and then combined. It can be seen that

by considering 3 principal parameters around 97% of variance of the original CAD model can be captured. For this study, 4 principal parameter are retained and PCA analysis of the combined model is used to further carry out the optimization studies.

Table 11: *Principal Component Analysis , Captured Variance*

Principal Parameter	Captured Variance		
	For Hull	For Tunnel	Combined
1	56.78	77.58	51.00
2	82.04	92.56	81.54
3	98.03	97.56	97.10
4	98.67	98.65	97.92
5	99.10	99.16	98.41
6	99.34	99.52	98.76
7	99.46	99.77	98.96

With the reduced KLE model, design of experiment (DOE) studies are carried out using SOBOL algorithm. The optimizer actually used 4 principal parameters as the design variables and spread it throughout the design space. These principal parameters are back transformed to actual design space to generate a CAD model using linear back transformation. Figure 52 highlights the results of the SOBOL runs carried out for KLE model. In Appendix E , correlation plots of KLE model is shown. The correlations plots highlights same correlations shown by the full PCA model, but with relatively less degrees of freedom and thus less number of designs. The reduced KLE model can be used to perform T-search with principal parameters and is expected to converge faster for only 4 variable. However, KLE based T-search is out of the scope of this project.

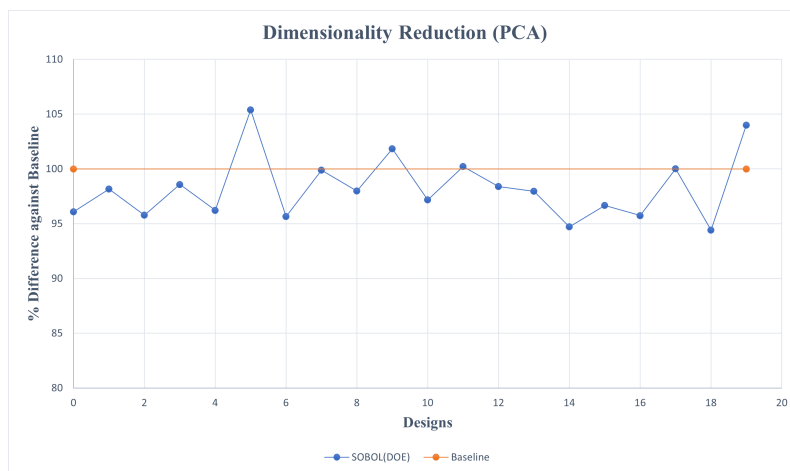


Figure 52: *Design of Experiment of Reduced (KLE) Model*

4.5 Comparison of Obtained Results

Having described different results obtained from various optimization methods, it is also essential to compare each of them. The comparison is carried out in terms of the efforts needed to obtain the optimum versus the quality of the optimized design. This section presents the comparison of obtained optimized designs, for both simplified setup and appended hull model with finer mesh.

4.5.1 Optimization Results for Simplified Model

Before proceeding with the comparison of obtained designs, the optimization framework is extended to better analyze the design space and to search for the global optimum. With the very fast optimization time of the trained surrogate model, it is possible to run several T-search from various designs of SOBOL that are already performing better. Figure 53 presents T-search from various starting points using surrogate model.

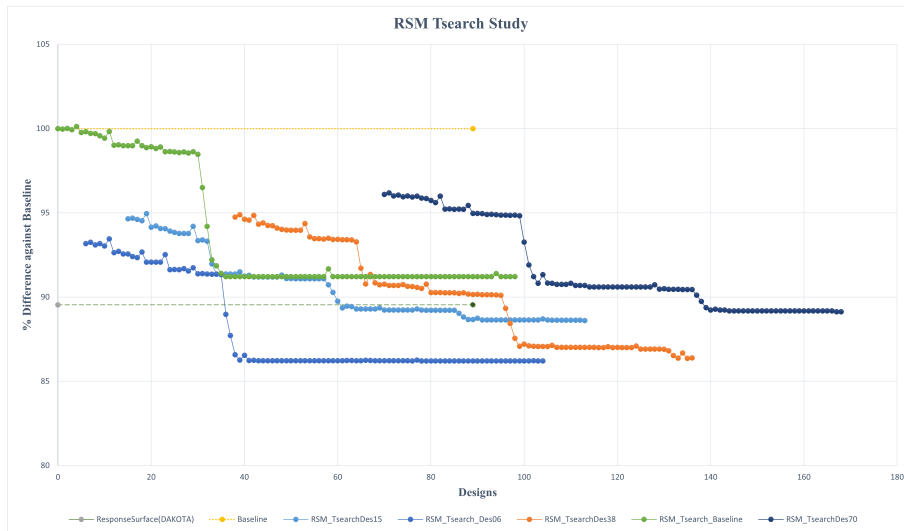


Figure 53: *T-search from various designs - Using Surrogate Model*

All the other optimized designs taken from SOBOL, KLE or DAKOTA were validated or computed with simplified CFD model. To make a good comparison and to check the validity of the trained surrogate model, optimized designs from several T-search are validated with CFD computations. To do that, each of the best converged design from Figure 53 is taken and CFD computations are performed with the automated setup. The results of this study is given in Table 12. Indicated results shows the behavior of the surrogate model which tries to over-predicts the improvement for each of the design. It is also interesting to see that with CFD model, other than the study that starts from the baseline, all the other optimization

tasks have shown almost same percentage difference. Improvement of around 10-11 % is given by each of the T-search, starting from various initial designs. Similar orders of improvement is given by DAKOTA response surface model, highlighting the possible presence of global optimum around this location.

Table 12: *Validation of Surrogate-Based T-search with CFD*

RSM Studies Results	% Improvement	
	With Kriging Model	With CFD Model
Starting from Baseline	91.21	93.13
Starting from Des0006	86.21	88.91
Starting from Des0015	88.11	90.05
Starting from Des0038	86.36	89.36
Starting from Des0070	89.13	90.39

Out of all these Surrogate based T-search designs, only one of them is chosen for the final validation and comparison with other designs. While looking at the above table, it seems preferable to take the results of Des0006 or Des0038. Nevertheless, as mentioned earlier the present optimization is a single-objective optimization focusing on the minimization of resistance only. This is directly link with the maximization of Lift Forces. Taking this into account, the optimizer goes into direction to maximize the surface area to create maximum lift forces. Thus, creating designs which are good for power reduction but have poor see-keeping performances. As see-keeping and stability analysis is out of the scope of this work, the designs which looks flatter are removed from the optimized set of design.

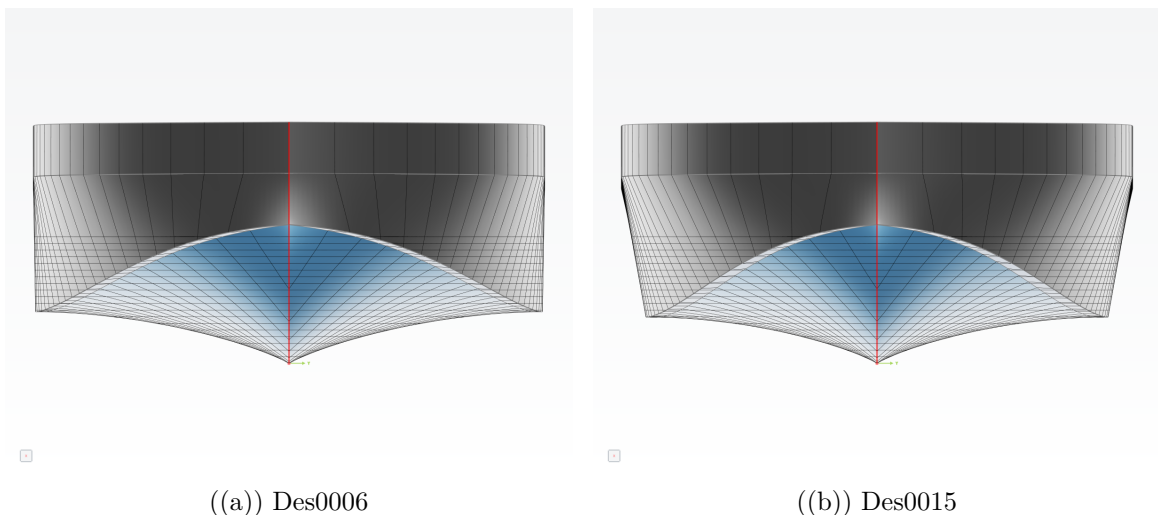


Figure 54: *Comparison of two designs from T-search - Front View*

Table 13 highlights the set of best designs obtained from various methods. Results of surrogate models are already validated with CFD computations. Hence, all the

obtained results can be compared with respect to optimization gain and corresponding computational time associated with the optimization process. Along with the table, an explanation of each obtained design is given here.

- 1st Optimized Design, also termed as new baseline for the optimization runs. This design is the result of manipulating the tunnel geometry based on intuitions to reduce wave making resistance, and shifting LCG towards aft to realize the potential gain in terms of total resistance reduction.
- 2nd Optimized Design, comes from the resulting Design of Experiment (SOBOL) analysis. By doing DOE analysis, some designs out-performing the baseline were identified and the best out of them is taken for validation purposes.
- 3rd Optimized Design, utilizes the best of the previous SOBOL runs and start a deterministic Tangent Search (T-search) to identify nearest local optimum.
- 4th Optimized Design, uses Response Surface Model to create a response surface and predict the output using genetic algorithms. It also utilizes the data set created from SOBOL runs.
- 5th Optimized Design, using the generated CFD data, a machine learning model is trained to perform deterministic optimization. The process of kriging is used and the trained model is much faster as compared to CFD computations, which were utilized by 3rd optimized design.
- 6th Optimized Design, utilized the reduced dimensional KLE based DOE analysis. With the reduced parameters, the requirement of testing several designs has been reduced to few designs. With few design variables or principal parameters, complete design space is represented and the best design is taken out of all designs.
- 7th Optimized Design, uses the reduced dimensional DOE data set to repeat the same procedure of 4th best design.

Eventhough, these tested designs represents simplified model without appendages and relatively coarser grid but the obtained results gives a good estimate of the actual model results. This is because optimization is always a relative task with respect to a fixed observation or design. By doing simplification and utilizing diligent optimization and Machine learning algorithms, around 10% of reduction in propeller thrust is highlighted. From Table 13, time taken for each optimization setup can be seen. Most of the response surface and ML models requires a training set so that to

make prediction of the objective function. Therefore, performing DOE analysis takes most part of the optimization process with almost 200 Hrs (for computations only) in this case. Depending on computational resources, design space can be reduced using KLE expansion as shown previously. By doing so, with less expense of computational resources a good design candidate can be found as in 6th or 7th design. It also comes with the price of relatively lower improvement in the performance as compared to full model.

Table 13: *Optimization Results for Simplified Model*

Optimized Design	Optimization Methods	Propeller Thrust (N)	Difference (%)	Time Taken (Hrs)
1st	New Baseline for Optimization	436.84	100	2.3
2nd	Design of Exploration (SOBOL)	413.42	94.64	207
3rd	Tsearch from 2nd	401.88	92.00	80.5
4th	DAKOTA based on SOBOL	391.12	89.53	2.3 + 207 (Data set)
5th	Tsearch-RSM	393.36	90.05	2.3 + 207 (Data set)
6th	Design of Exploration (SOBOL) - KLE	415.56	95.13	46
7th	DAKOTA - based on KLE	424.32	97.13	2.3 + 46 (Data set)

4.5.2 Optimization Gain for Appended Model

Previously shown results of the simplified model gives best performing design candidates for each methods. The simplification of the model by removing appendages and using coarser grid, is based on the assumption that both of these have an 'added' effect on the objective function. Therefore, relative improvement against a fixed design baseline should be same for appended and simplified model. This assumption was useful in decreasing the turnaround time by a factor of 2 given in Table 13. Without these assumptions, the time taken for the optimizations would be 2 times the mentioned time.

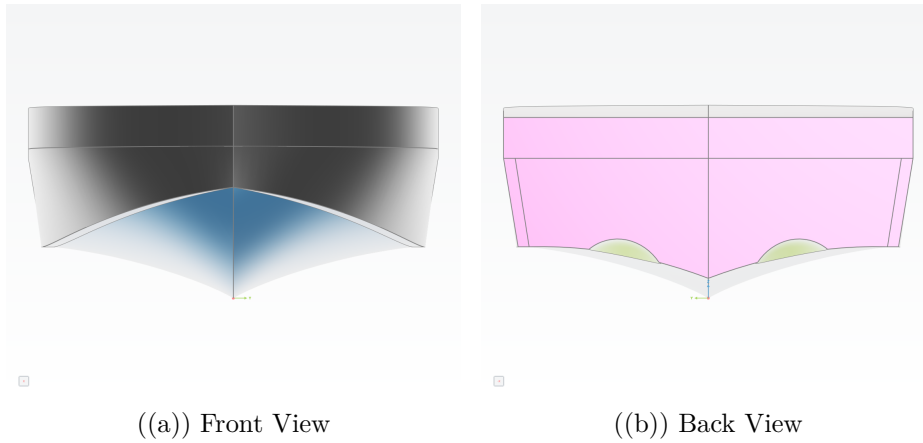
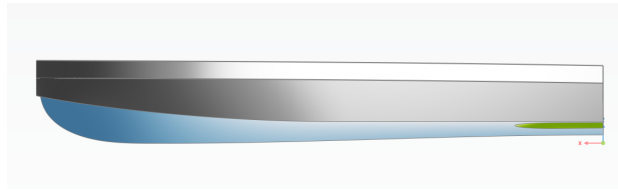
To check the validity of these assumptions and test different design candidates. Original baseline which was validated against tank tests is compared with all 7 best possible design candidates. In Table 14, the comparison is made with 'Original Baseline' with initial LCG position. First optimized design which shows 4.92% improvement in Thrust deduction, is the 'New Baseline' for previous runs. All the other optimized design candidates have shown same order of improvement as with the simplified model. Optimization gains for this study using different methods varies from 5 to 15 % reduction in thrust and hence engine power.

Based on the observed results, DAKOTA response surface based optimization outperforms different candidates with 15.77% improvement with respect to baseline. Pictures of the best design candidate is given in Figure 55, 56 and 57. Different views of other design candidates are given in Appendix F. It is interesting to see that all of these design variants computed from entirely different methods, have

Table 14: *Optimization Results for Fully Appended Model with Fine Mesh*

	Original Baseline	Optimized Design							Units
		1st	2nd	3rd	4th	5th	6th	7th	
Thrust	520.4	494.78	448.6	440.76	434.64	438.34	452.04	487.3	N
RPMs	2280.29	2255.47	2204.2	2205.83	2205.12	2199.32	2206.72	2230.34	/s
Torque	24.44	23.46	21.42	21.196	20.9644	21.0506	21.54	22.84	N.m
Power	2.9180	2.7705	2.4721	2.4481	2.4205	2.4241	2.4888	2.6673	kW/motor
Pitch	3.67	4.214	3.83	4.57	4.556	5.01	3.65	4.19	deg
Heave	0.0792	0.0975	0.09	0.1038	0.1047	0.1134	0.0871	0.1267	m
LCG	1.504	1.354	1.354	1.354	1.354	1.354	1.354	1.354	m
% Improvement	-	4.92	13.80	15.30	16.48	15.77	13.14	6.36	%

similar characteristics. This involves, presence of rocker at the aft, much flatter sides of the transom besides tunnel, convexity of the keel line near bow part, and smaller but shallow tunnels as shown.

Figure 55: *Best Optimized Design Candidate - Using DAKOTA Response Surface*Figure 56: *Best Optimized Design Candidate - Side View*Figure 57: *Best Optimized Design Candidate - Bottom View*

Chapter 5

Conclusion & Future Work

The motivation behind this thesis was to present a comprehensive study for the simulation driven design of a High Speed Planing Craft optimization. Not only that, but to introduce methods for the faster turn around time of simulation driven design of a complex problem of planing hulls. The proposed methodology and subsequent faster optimization techniques can be applied to any other case of SDD with minor relevant changes.

Speeding-up the optimization tasks does not necessarily comes from faster optimization strategies. But, diligently employed CFD methods for efficient and accurate predictions in a shorter time, also plays an important role. This is true, because for any data-driven optimization task large amount of data showing the effect of design variables on the objective function is required. In this case, efficient CFD methods employed for faster CFD predictions of the objective function is shown. Results are verified using grid convergence studies and validated against tank tests results. Presented results are found to have good convergence as well as validation against experimental data that is, around 1 % difference of drag force and propeller thrust.

Automated software connection for faster optimization task is also one of the essential method for speeding up SDD. Before starting the conventional optimization runs, simplification of the numerical setup is exercised. It is shown that by using a very simplified geometry along with a relatively coarser grid simplified model is 2 times faster as compared to actual complete setup. It is also essential to identify that the importance of relative improvement against a baseline is more important for the optimization task rather than quantifying the actual improvement at initial stage. After finding a set of relatively improved designs, back transformation to actual hull model helps in quantifying the actual improvement for the design.

A set of optimized designs using different optimization methods are presented. These optimization tasks utilizes various Design of Experiment and Exploitation tools. These tasks are applied to fully parametric model as well as reduced dimensional KLE model. Calculation of objective function or propeller thrust is carried out first by using CFD, then by using data-driven algorithms trained on CFD data.

Performed set of optimized designs have shown improvement of between 5-15 % in propeller thrust reduction. The amount of propeller thrust reduction that can be achieved depends on the amount of time available for the optimization runs as for any industrial applications. With limited computational resources available, KLE based optimization can be carried out to produce an optimized design with few % improvement (Optimized Design 6th and 7th in this case). If enough computational resources are available, more detailed data-driven and response surface optimization tasks presents good improvement in design performance. With designs 4th and 5th shows the presence of global optimum of the optimization problem.

Speeding-up of simulation driven designs are successfully employed for the case of high-speed planing hulls. Presented results shows significant improvements in the propeller thrust reduction for planing vessels starting from the initial baseline. A set of optimized design resulting from various data-driven and AI-based optimization strategies can be selected for production and validation in tank tests. Current work of optimization and simulation-driven design can be extended for any other complex application with appropriate relevant changes.

5.1 Future Work

Although various optimization and speeding-up methods of SDD are already shown in this work. Nevertheless, optimization is always an ongoing process. Some of the future prospects of this work is to study following topics.

Using various deterministic optimization strategies other than T-search to find good local or global optimum, and to compare the optimization time. Also, the work of KLE based optimization, can be extended to perform design of exploitation after SOBOL (DOE) analysis.

The concept of adjoint simulations is another strategy that is expected to be much faster and efficient in terms of optimization. It uses calculation of sensitivities and a primal solution to optimize the design. Though it is efficient but creating a CFD code for adjoint simulations of movable (overset) grid is still a challenging task. The use of parametric model with adjoint simulations, so called parametric-adjoint simulations is another task to be studied in this context.

Bibliography

- Albert, S. et al. (2016). “Hydrodynamic Optimization of a Power Boat in the Cloud”. In: *High-Performance Marine Vehicles (HIPER 2016)*, Cortona, Italy.
- Bertram, Volker (2012). “Chapter 3 - Resistance and Propulsion”. In: *Practical Ship Hydrodynamics (Second Edition)*. Ed. by Volker Bertram. Second Edition. Oxford: Butterworth-Heinemann, pp. 73–141. ISBN: 978-0-08-097150-6.
- Harries, S. (2015). “Practical Shape Optimization using CFD”. In: *Whitepaper*, Potsdam, Germany.
- Harries, S. and C. Abt (2019a). “CAESES—The HOLISHIP Platform for Process Integration and Design Optimization”. In: *A Holistic Approach to Ship Design: Volume 1: Optimisation of Ship Design and Operation for Life Cycle*. Ed. by Apostolos Papanikolaou. Cham: Springer International Publishing, pp. 247–293. ISBN: 978-3-030-02810-7.
- (2019b). “Faster turn-around times for the design and optimization of functional surfaces”. In: *Ocean Engineering* 193, p. 106470. ISSN: 0029-8018.
- Harries, S., C. Abt, and M. Brenner (2019). “Upfront CAD—Parametric Modeling Techniques for Shape Optimization”. In: *Advances in Evolutionary and Deterministic Methods for Design, Optimization and Control in Engineering and Sciences*. Ed. by Edmondo Minisci et al. Cham: Springer International Publishing, pp. 191–211. ISBN: 978-3-319-89988-6.
- Harries, S. and S. Uharek (2021). “Application of Radial Basis Functions for Partially-Parametric Modeling and Principal Component Analysis for Faster Hydrodynamic Optimization of a Catamaran”. In: *Journal of Marine Science and Engineering* 9.10. ISSN: 2077-1312.
- Hasubek, B. and S. Harries (2017). “Simulation-Driven Design of Sailing Yachts and Motor Boats”. In: *PVII International Conference on Computational Methods in Marine Engineering (MARINE 2017)*, Nantes, France.
- “International Towing Tank Conference” (n.d.). In: ()

- Kim, Dong Jin et al. (2013). “Design of high-speed planing hulls for the improvement of resistance and seakeeping performance”. In: *International Journal of Naval Architecture and Ocean Engineering* 5.1, pp. 161–177. ISSN: 2092-6782.
- Roshan, Fatemeh et al. (Mar. 2020). “Hydrodynamic characteristics of tunneled planing hulls in calm water”. In: *Brodogradnja* 71, pp. 19–38.
- Savitsky, Daniel (1964). “Hydrodynamic Design of Planing Hulls”. In: *Marine technology* 1, pp. 71–95.
- Wheeler, Miles P., Konstantin I. Matveev, et al. (2021). “Numerical Study of Hydrodynamics of Heavily Loaded Hard-Chine Hulls in Calm Water”. In: *Journal of Marine Science and Engineering* 9.2. ISSN: 2077-1312.
- Using VOF Slip Velocity to Improve Productivity of Planing Hull CFD Simulations* (Oct. 2021). Vol. Day 1 Tue, October 26, 2021. SNAME International Conference on Fast Sea Transportation. D011S002R002.
- Xing, Tao and Frederick Stern (June 2010). “Factors of Safety for Richardson Extrapolation”. In: *Journal of Fluids Engineering* 132.6. 061403. ISSN: 0098-2202.
- Zadow, H. Von et al. (2019). “Methods of Simulation-driven Design in the Maritime Industry”. In: *Proceedings of the 6th International Conference on Ship and Offshore Technology (ICSOT), Kharagpur, India.*

Appendices

Appendix A

Numerical Setup

Slip velocity blending direction is given by,

$$B_d = \min\left(\left(\frac{\textit{Wall Distance}}{1.5 \textit{ Prism Layer Thickness}}\right)^3, 1\right) \quad (\text{A.1})$$

Force balance if the bubble is considered as sphere,

$$\frac{\pi d^3 \Delta \rho g}{6} = \frac{C_d}{2} \rho_c u_t^2 \frac{\pi d^2}{4} \quad (\text{A.2})$$

Density of air-water mixture for VOF method,

$$\rho = \rho_{air} \beta + \rho_{water} (1 - \beta) \quad (\text{A.3})$$

Viscosity of air-water mixture using VOF method,

$$\mu = \mu_{air} \beta + \mu_{water} (1 - \beta) \quad (\text{A.4})$$

Governing equations for high resolution interface capturing scheme (HRIC) for VOF method,

$$\frac{\delta \rho}{\delta t} + \frac{\delta(\rho \mu_j)}{\delta x_j} = 0 \quad (\text{A.5})$$

$$\frac{\delta(\rho \mu_i)}{\delta t} + \frac{\delta(\rho \mu_i \mu_j)}{\delta x_j} = \frac{\delta \rho}{\delta x_i} + \frac{\delta \rho}{\delta x_i} \left[\mu \left(\frac{\delta u_i}{\delta x_j} + \frac{\delta u_j}{\delta x_i} + \frac{2}{3} \delta_{ij} \frac{\delta u_k}{\delta x_k} \right) \right] + \rho f_i \quad (\text{A.6})$$

$$\frac{\delta \beta}{\delta t} + \frac{\delta(\beta \mu_i)}{\delta x_i} = 0 \quad (\text{A.7})$$

Appendix B

Flowchart for PCA

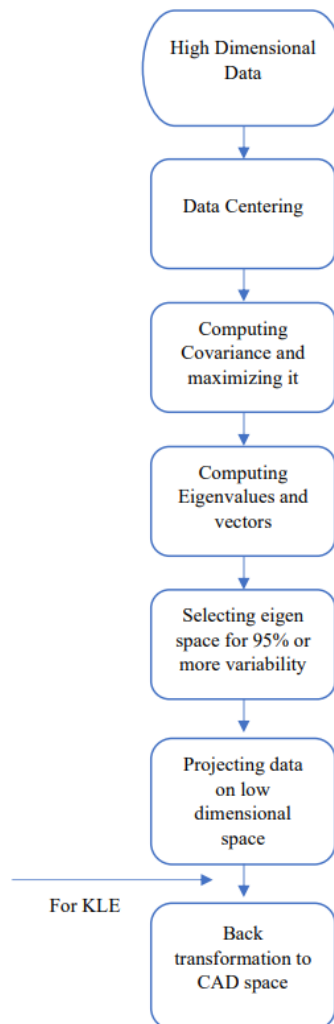


Figure 58: *Flowchart of the steps of PCA*

Appendix C

Wave Forcing Equation

Introducing wave forcing term at right hand side of momentum equation,

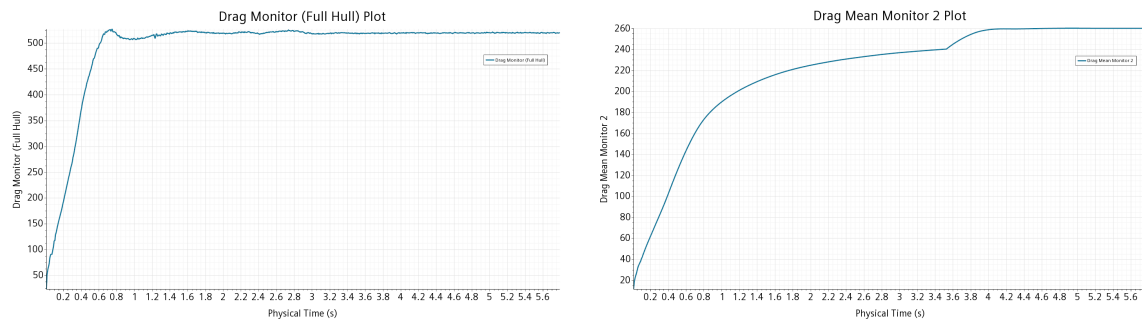
$$q_\phi = -\gamma\rho(\phi - \phi^*) \quad (\text{C.1})$$

Wave forcing coefficient γ is given by,

$$\text{Wave forcing coefficient } (\gamma) = -\gamma_o \cos^2\left(\frac{\pi x^*}{2}\right) \quad (\text{C.2})$$

Appendix D

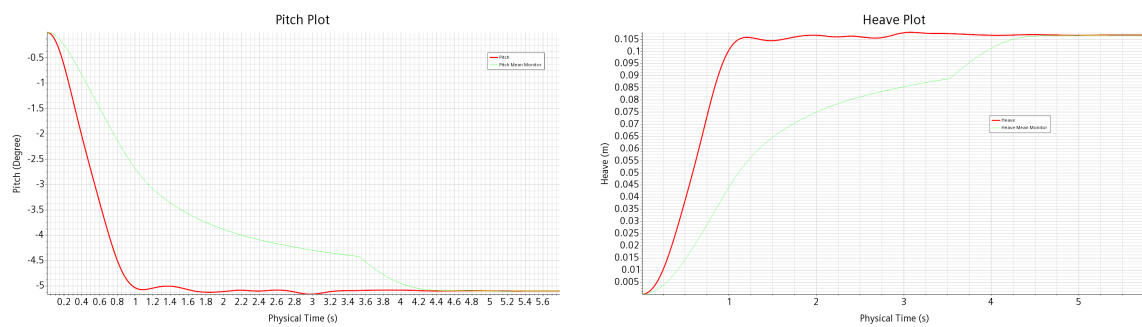
Convergence Histories



((a)) For Instantaneous Drag Force

((b)) For Mean Drag Force

Figure 59: *Convergence Histories for Drag Force*



((a)) For Pitch

((b)) For Heave

Figure 60: *Convergence Histories for Pitch and Heave*

Table 15: *Validation Studies at different Speeds*

Fr	Experimental Test				CFD			
	V (knots)	RT (N)	Trim (Deg)	Heave (cm)	V (knots)	RT (N)	Trim (Deg)	Heave (cm)
0.2612	5.29	80.91	0.28					
0.6790	13.75	318.19	3.46		13.75	316.90	3.28	0.90
0.8149	16.50	362.06	3.65		16.50	362.56	3.87	2.95
0.9507	19.25	403.47	3.92		19.25	411.99	4.58	5.17
1.0865	22.00	447.43	4.27		22.00	452.43	5.12	7.63
1.2223	24.75	481.70	4.34		24.75	485.82	5.19	9.41
1.3581	27.50	521.54	4.22	9.53	27.50	520.14	5.10	10.67
1.4940	30.25	560.32	4.19		30.25	556.39	4.95	11.61

Appendix E

Correlation Plots

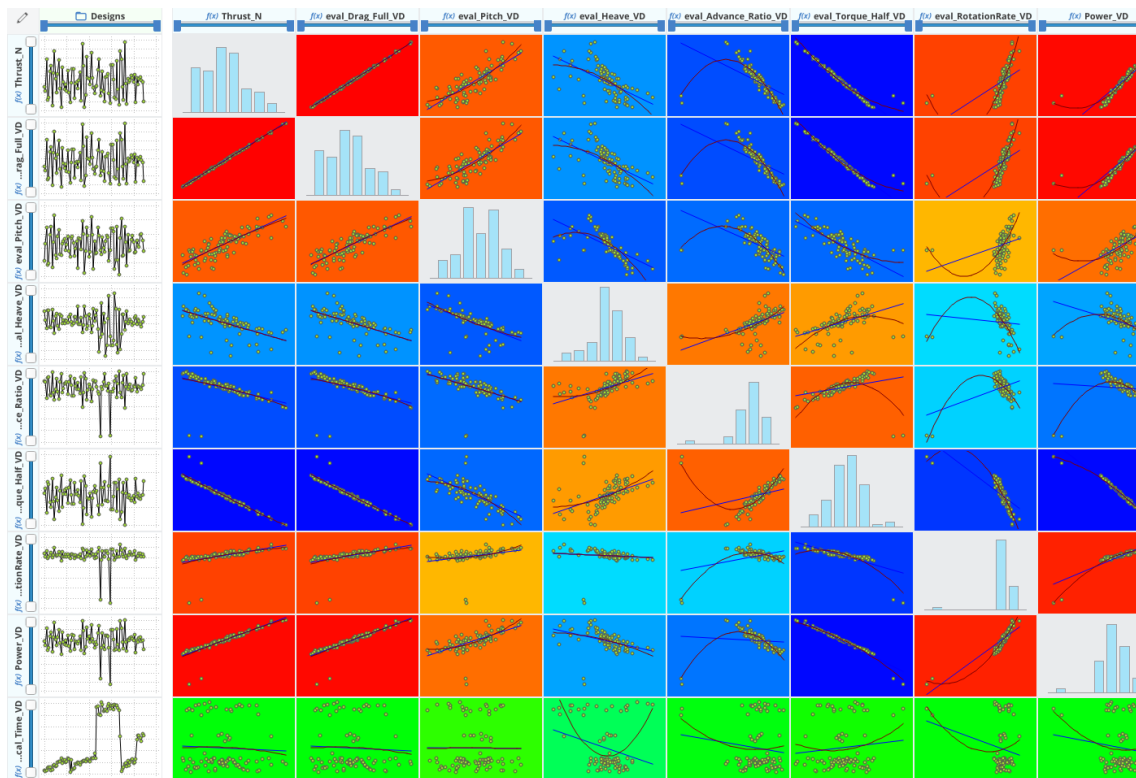


Figure 61: *Design of Experiment Analysis (SOBOL) - Correlations Plots*

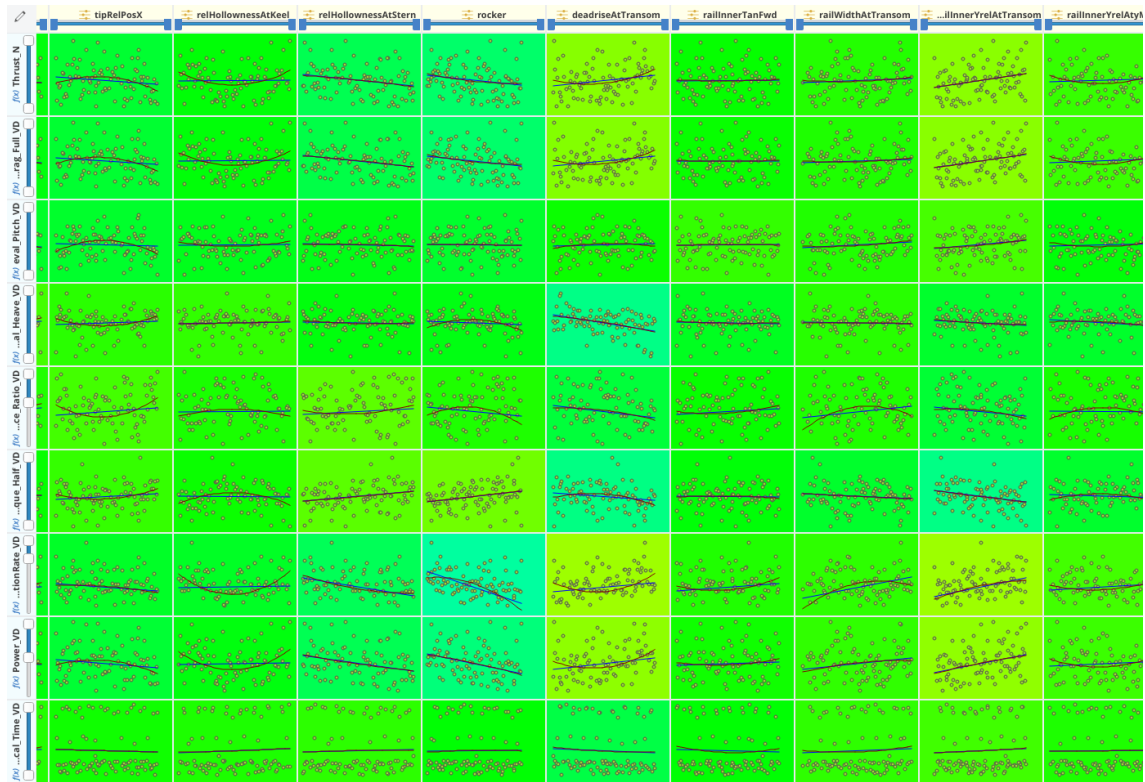


Figure 62: *Design of Experiment Analysis (SOBOL) - Correlations Plots*

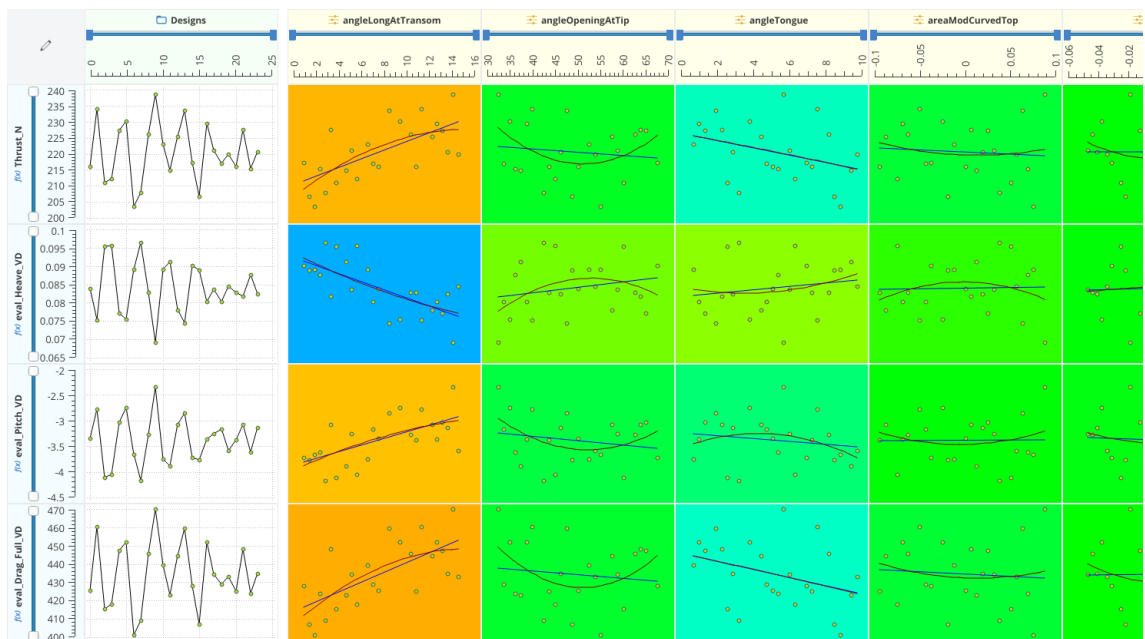
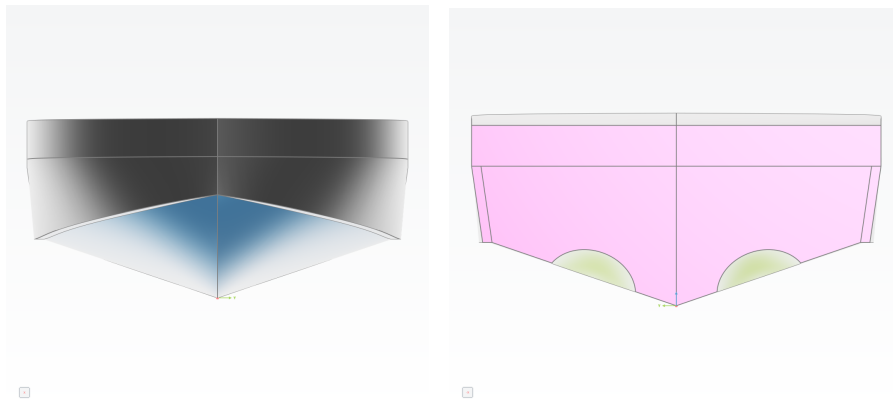


Figure 63: *Design of Experiment Analysis (SOBOL) - Correlations Plots - KLE*

Appendix F

Optimized Designs



((a)) Front View

((b)) Back View

Figure 64: *1st Optimized Design*

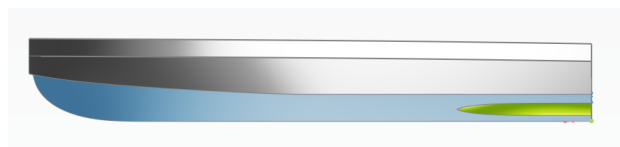


Figure 65: *1st Optimized Design - Side View*

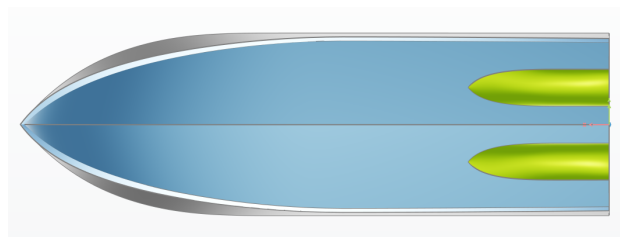


Figure 66: *1st Optimized Design - Bottom View*

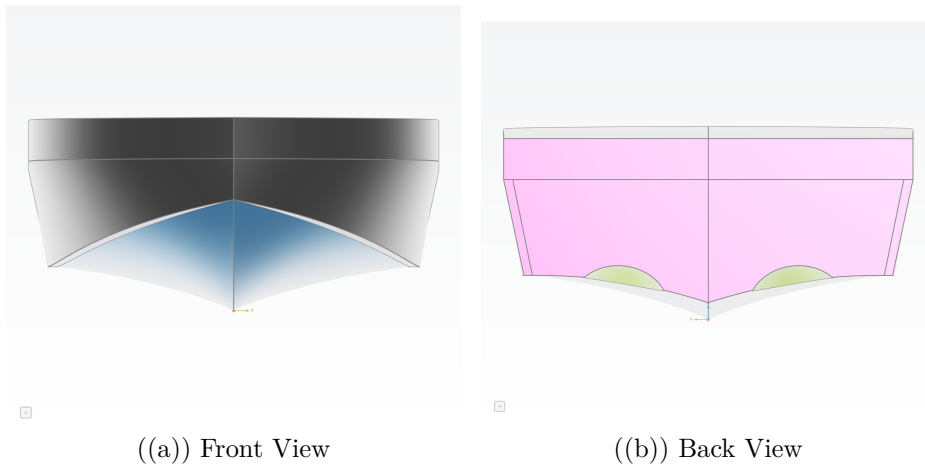


Figure 67: *2nd Optimized Design*

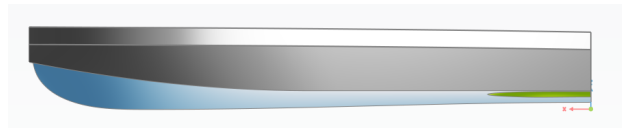


Figure 68: *2nd Optimized Design - Side View*

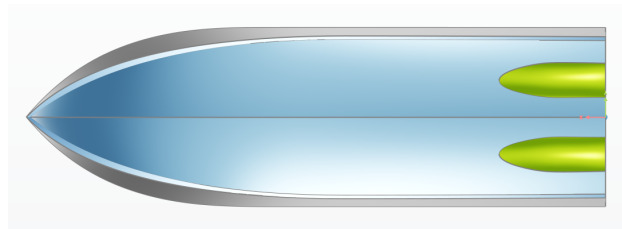


Figure 69: *2nd Optimized Design - Bottom View*

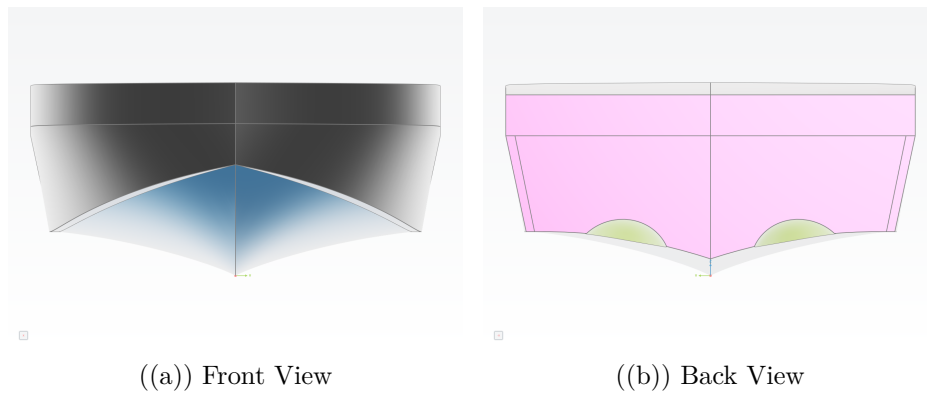


Figure 70: *3rd Optimized Design*

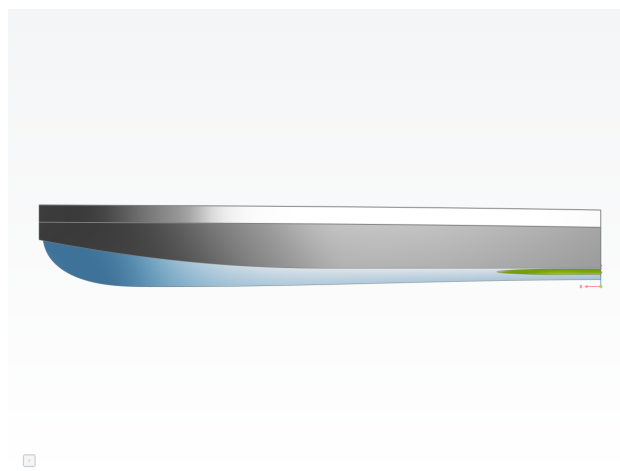


Figure 71: *3rd Optimized Design - Side View*

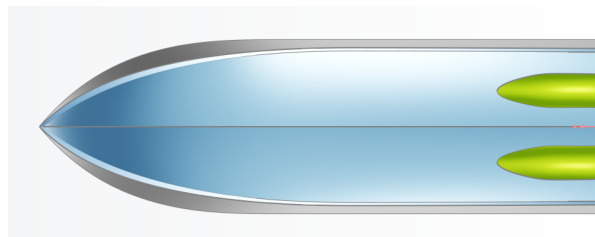


Figure 72: *3rd Optimized Design - Bottom View*

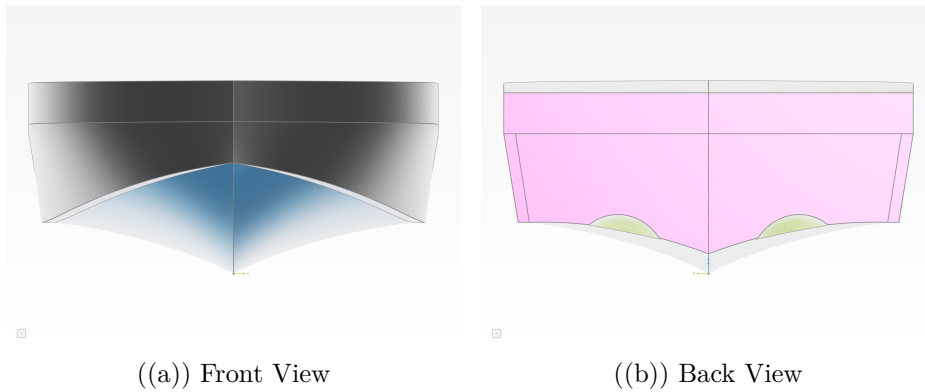


Figure 73: *5th Optimized Design*

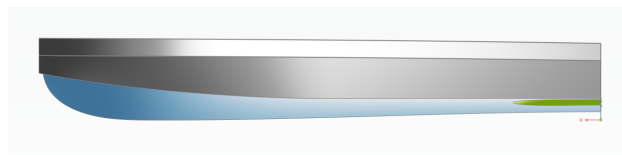


Figure 74: *5th Optimized Design - Side View*

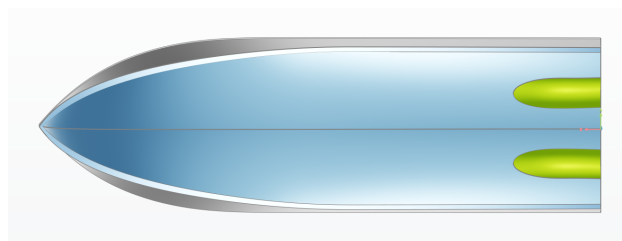
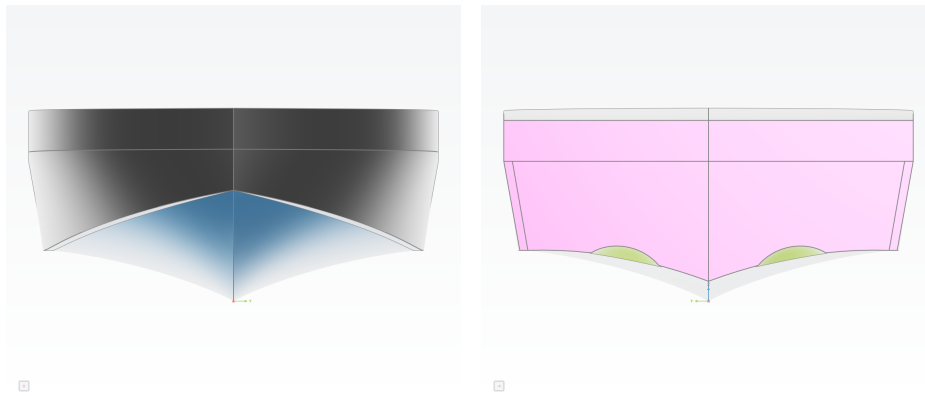


Figure 75: *5th Optimized Design - Bottom View*



((a)) Front View

((b)) Back View

Figure 76: *6th Optimized Design*

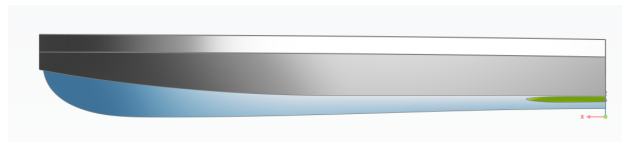


Figure 77: *6th Optimized Design - Side View*

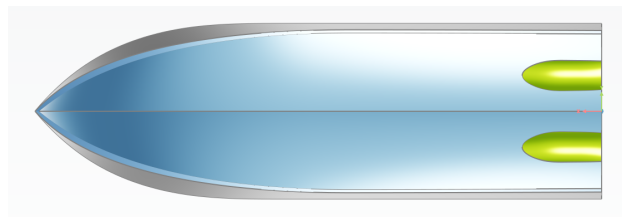


Figure 78: *6th Optimized Design - Bottom View*

Appendix G

Baseline Results at Design Speed

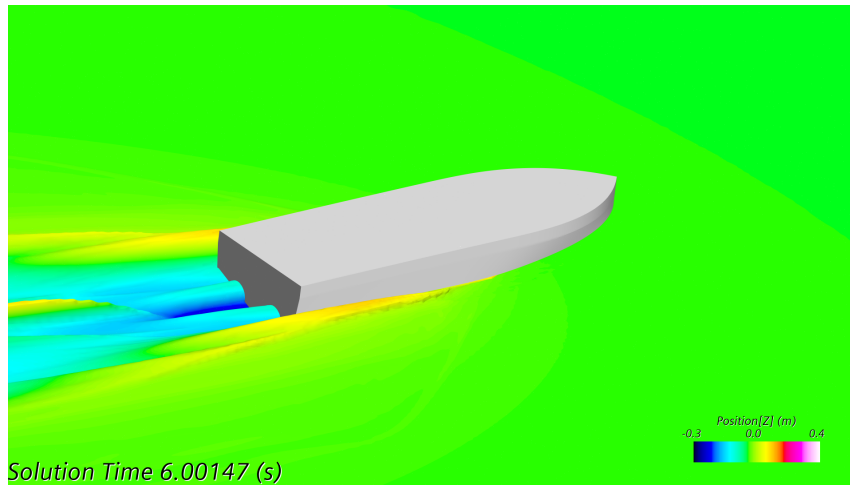


Figure 79: *Free Surface around the vessel*

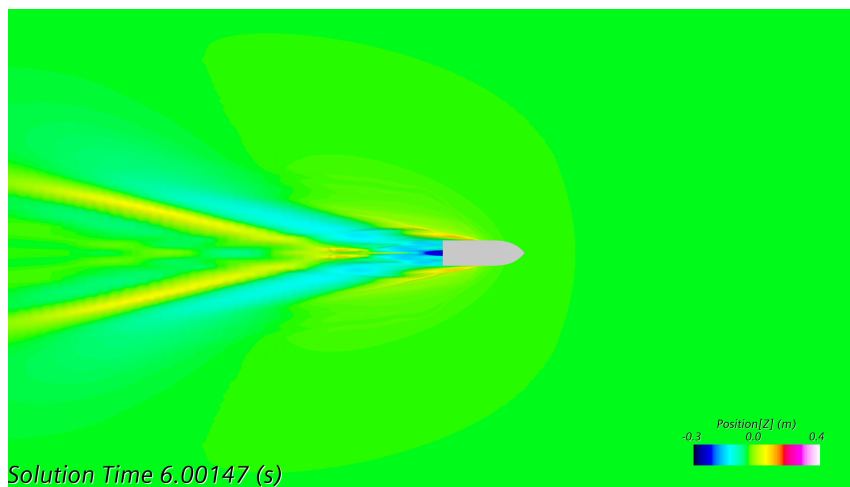


Figure 80: *Free Surface around the vessel*

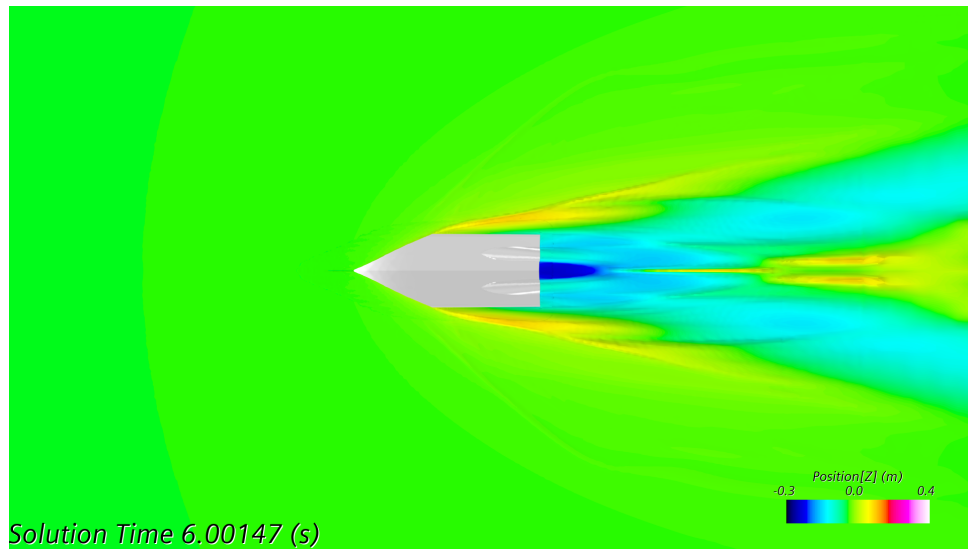


Figure 81: *Free Surface around the vessel*

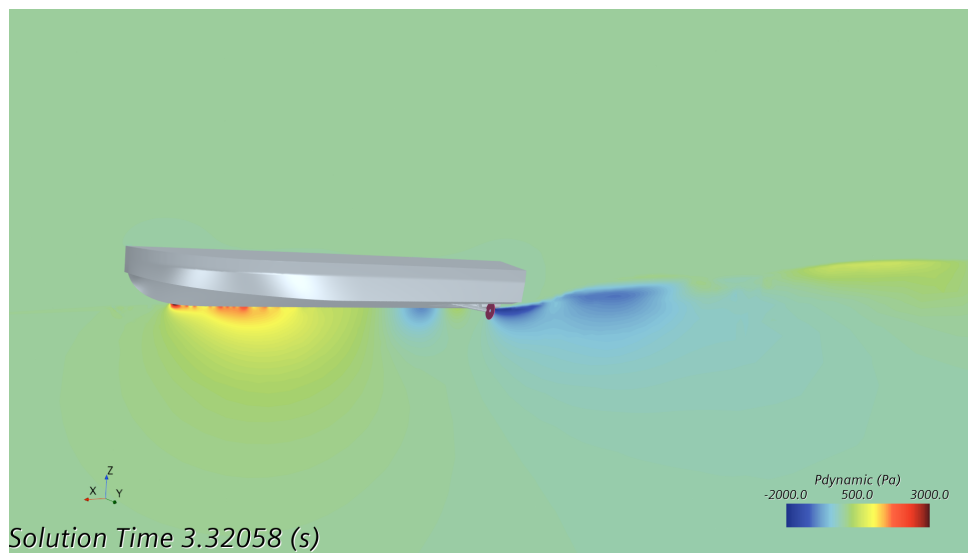


Figure 82: *Pressure distribution with propeller disk*

Appendix H

Data Filtering

Table 16: *Unfiltered Data for Surrogate Model*

# of Variants	CoP Value		Function Value	
	Kriging	ANN	Kriging	ANN
30	0.9049	0.613	218.42	221.36
35	0.8167		218.42	
40	0.8889	0.786	218.42	223.47
45	0.9142		218.42	
50	0.8499	0.7273	218.42	221.87
55	0.9168		218.42	
60	0.8589	0.6525	218.42	213.08
65	0.9041		218.42	
70	0.8604	0.6429	218.42	217.77
75	0.7673		218.42	
80	0.8267	0.518	218.42	215.63
85	0.8309		218.42	

Appendix I

Validation Studies for 1st Variant (New Baseline)

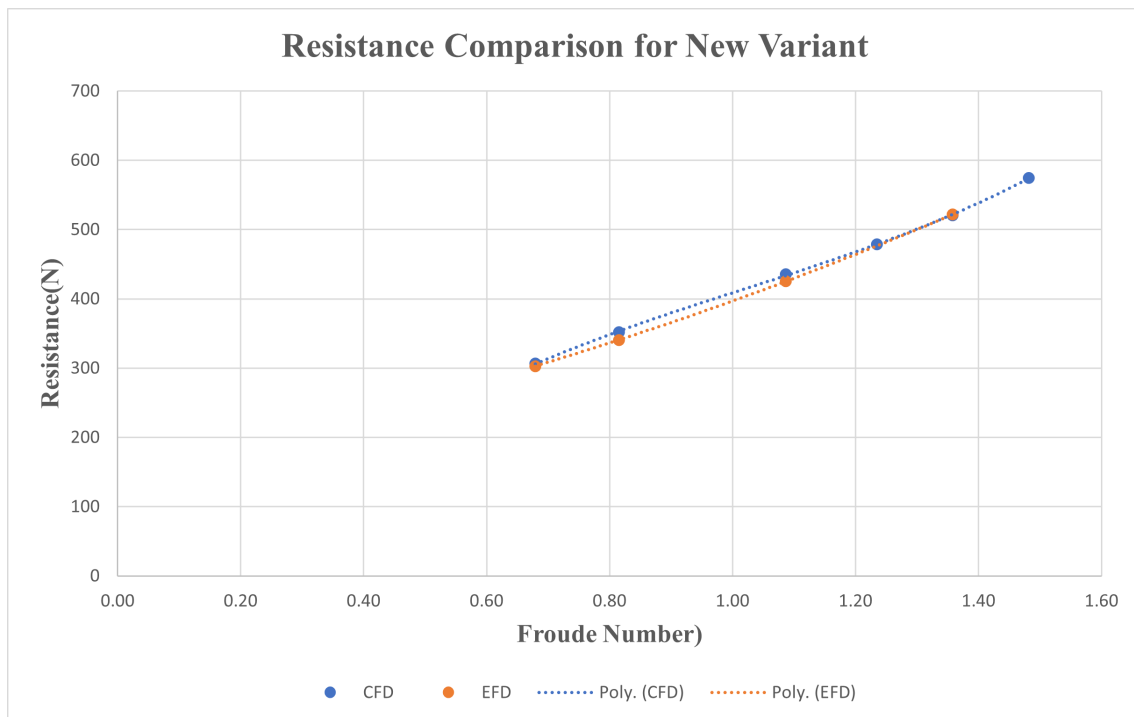


Figure 83: *Validation Studies New Variant - Resistance*



Figure 84: Validation Studies New Variant - Pitch

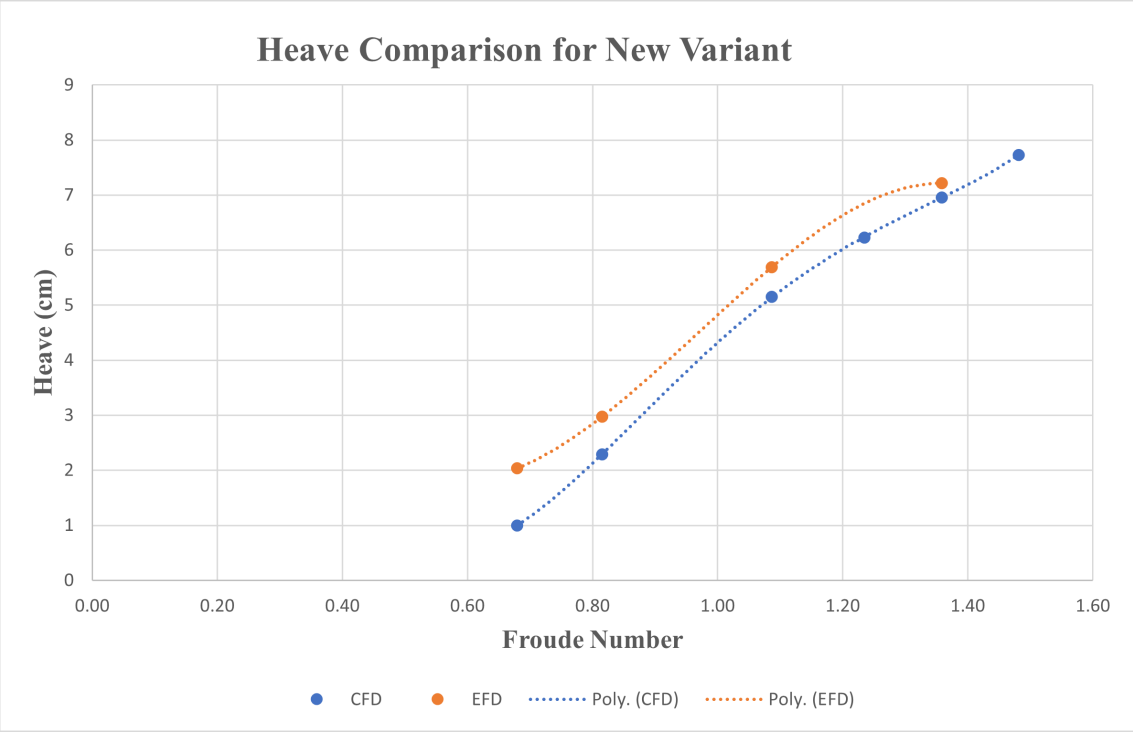


Figure 85: Validation Studies New Variant - Heave

Appendix J

Propeller-Open Water Characteristics

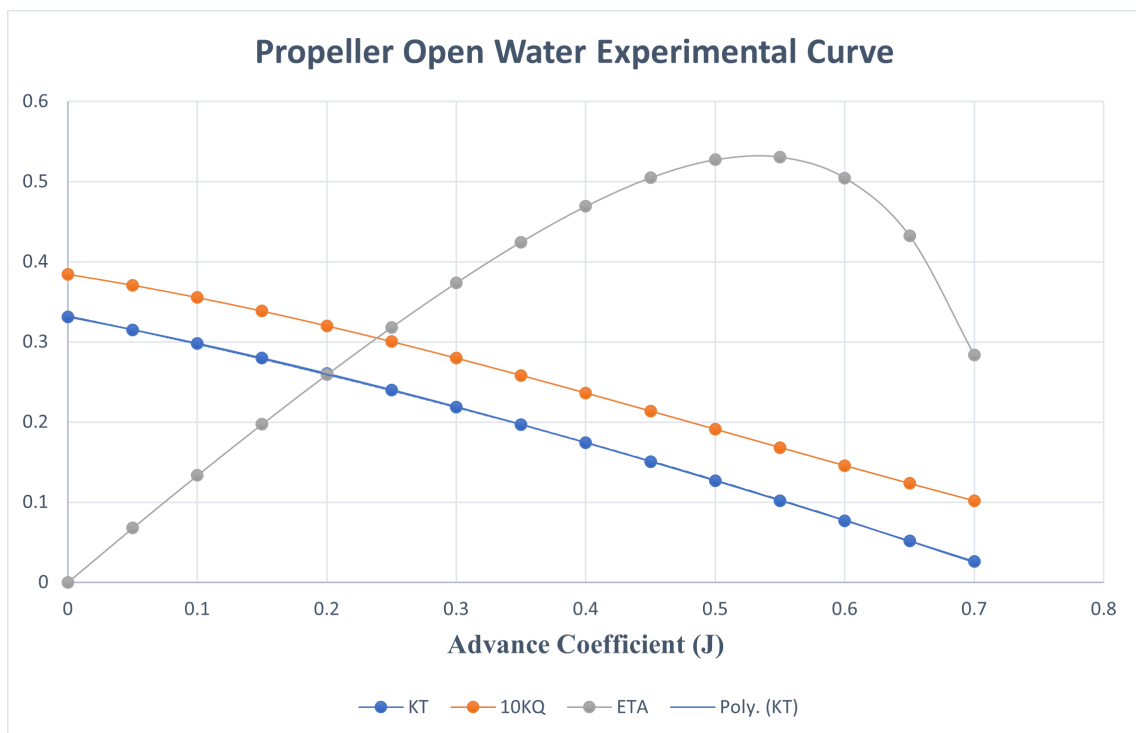


Figure 86: *Propeller Open Water Experimental Curves*